

Internal Representation, Not Clinical Knowledge: Where Apparent LLM Triage Failures Originate

David Fraile Navarro¹, Bernardino Como², Jialei Sheng³, Soundariya Ananthan⁴, Shlomo Berkovsky¹

¹Macquarie University, Sydney, Australia ²Politecnico di Bari, Bari, Italy

³NSW Health, Sydney, Australia ⁴Independent Researcher

david.frailenavarro@mq.edu.au, b.como@studenti.poliba.it, jialei.sheng@health.nsw.gov.au,

a.soundariya@gmail.com, shlomo.berkovsky@mq.edu.au

Correspondence: david.frailenavarro@mq.edu.au

Abstract

Patient-voiced clinical-triage benchmarks report high under-triage rates for consumer LLMs for constrained multiple-choice output, yet the same cases score differently with free-text. We ask whether output format changes the model’s *clinical representation* or only the *mapping* from a preserved representation to an answer. Using sparse-autoencoder (SAE) features in Gemma 3 4B/12B IT and Qwen3-8B, we find the same medical features fire on the shared clinical narrative under both formats but go silent at the multiple-choice decision token in all the cases at every model. Three independent methods (natural-language autoencoder verbalization, decision-token logit attribution, and top-feature characterization) agree that scaffold and format features, but not medical features, drive the decision logits. Behaviorally, the multiple-choice penalty inverts under both structured and natural-language input, option-order shuffle rules out positional bias, and the gap is dominated by off-by-one decision (the model picks an adjacent acuity letter to the gold answer) rather than knowledge failure. Thus, the failure originates in the output format and not in the clinical representation.

1 Introduction

Large language models (LLMs) are increasingly evaluated for clinical reasoning. With appropriate alignment they reach near-clinician agreement on medical questions (Singhal et al., 2023), suggesting that LLMs encode substantial clinical knowledge. Recent work, however, reports high failure rates on triage specifically (Ramaswamy et al., 2026): a consumer-LLM clinical-triage benchmark (evaluating ChatGPT on patient-voiced vignettes) demonstrated a 51.6% emergency-case under-triage rate, an alarming headline cited as evidence that current LLMs may be unsafe for clinical triage. A behavioral replication shows that changing the *scaffolding*, i.e., rephrasing structured triage cases into

natural-language text with free-text output, eliminates a substantial portion of the reported failures (Fraile Navarro et al., 2026), consistent with a broader literature on prompt-format and multiple-choice sensitivity in LLM benchmarks (Zheng et al., 2024; Pezeshkpour and Hruschka, 2024; Sclar et al., 2024). The triage failures are therefore at least partly a function of the evaluation setting rather than the model performance.

This raises a question that behavior alone cannot answer: *where does the failure originate from?* Two hypotheses are plausible. **Encoding-shift hypothesis:** under the multiple-choice format, the model fails to access its clinical knowledge, as the multiple-choice scaffold (answers appended to the question) induces the failure, with the representation of the clinical case becoming different from the free-text generation. **Output-mapping hypothesis:** prompt format changes how the model maps an already-formed clinical representation onto the final answer; the clinical encoding is preserved, and the benchmark measures the output stage correctness rather than the clinical reasoning.

This distinction has well-established conceptual precedent (Burns et al., 2023; Kadavath et al., 2022; Turpin et al., 2023). Concurrent work in clinical triage specifically documents a 53-pp knowledge-action gap on Qwen 2.5 7B Instruct, with four mechanistic interventions, including SAE feature steering, failing to reliably correct it (Basu et al., 2026). We ask a different, more specific question: where does the gap originate from when output format is varied while the clinical-content portion of the prompt is held unchanged?

Contributions. In this work, we investigate where the apparent multiple-choice penalty in LLM clinical triage originates. We combine SAE features, natural-language autoencoders, linear probes, and behavioral decomposition across three instruction-tuned LLMs from two families to localize the format effect. Our contributions are:

- We show that medical content is preserved across multiple-choice and free-text formats: the identified medical features peak on the clinical narrative in both cases.
- We localize the multiple-choice effect to a representational shift at the decision token. At the hidden state that drives the answer selection, medical features go silent and scaffold features dominate. Three independent methods (SAE logit attribution, decision-token top-feature analysis, and natural-language autoencoder verbalization) support this finding.
- We decompose the performance gap between multiple-choice and free-text formats into miscalibration (dominates the measured gap at every model) and deferral (separate label-space concern not contributing to this gap), and rule out positional bias via option-order shuffles.
- We deploy a linear-probe framework to predict what cases will flip correctness between formats from source-format hidden states alone. We also report a Constraint-First ablation suggesting that the position of the constraint relative to the generation point contributes substantially to the representational shift, beyond the effect of its mere presence.

Across Gemma 3 4B IT, Gemma 3 12B IT, and Qwen3-8B, the format effect localizes to scaffold features at the decision token while medical content remains intact upstream. This is consistent with output-stage mapping rather than degraded clinical reasoning as the source of the apparent failure rate. Code, data, and analysis scripts to reproduce all experiments are available at https://github.com/dafraile/SAE_mad.

2 Background and Related Work

Triage disposition and medical diagnosis are distinct cognitive tasks operating under different information states and error tolerances (Yancey and O’Rourke, 2023). Triage functions as an initial working hypothesis formed under time pressure and informational scarcity, where the dominant strategy is to rule in risk by erring toward higher acuity, with an accepted error rate that is expected to resolve as clinical context accumulates. Diagnosis then inherits triage as a prior to be tested rather than a conclusion to be accepted, progressively ruling out competing explanations as history, examination, and investigation accumulate. Therefore,

for LLM evaluation the reasoning task under evaluation is an initial acuity disposition under sparse information, not a final diagnosis.

Notable previous LLM evaluation in Clinical AI include Med-PaLM, establishing that LLMs encode substantial clinical knowledge (Singhal et al., 2023, 2025). Specific benchmarks have probed failure modes of consumer-facing LLMs on patient-voiced clinical-triage vignettes (Ramaswamy et al., 2026). Behavioral replications by (Fraile Navarro et al., 2026) indicate that constrained-output evaluation is a major contributor to the apparent failure rates medical triaging. Concurrent mechanistic work on the same task documents a 53-pp knowledge-action gap on Qwen 2.5 7B Instruct and shows four mechanistic interventions fail to reliably correct it (Basu et al., 2026); our complementary localization varies output format while holding the patient vignette verbatim, showing *where* the format difference lives rather than attempting to fix it by intervention.

3 Methods

3.1 Dataset

We use all 60 clinical vignettes from the replication corpus of (Fraile Navarro et al., 2026), reconstructed from the clinical-triage benchmark of (Ramaswamy et al., 2026). The corpus spans input format (structured vignettes or naturalistic/conversational symptom depictions) and output formats either (multiple-choice or free-text) in a 2×2 factorial, yielding four conditions: **SL** (structured + multiple-choice), **NL** (natural + multiple-choice), **SF** (structured + free-text), and **NF** (natural + free-text). In our condition codes the first letter denotes input (**S**tructured or **N**atural), and the second letter denotes output (**L**etter for forced-letter multiple-choice, **F** for free-text). Throughout, ‘multiple-choice’ refers to prompts that select a 4-option A-D single-letter response; we call this appended instruction block the **multiple-choice scaffold**. Within each input format the forced-letter and free-text conditions are byte-identical in clinical content (NL-NF at 1033 characters/case) and differ only in whether the multiple-choice scaffold (50–60 tokens) is appended. NL-NF and SL-SF therefore each isolate output format at a fixed input. Mechanistic analyses use the NL-NF pair throughout; SL-SF appears as a behavioral robustness check in Section 4.1 and as an input-style mechanistic robustness check in Appendix X. Out-

put gold labels follow the source benchmark’s four care tiers (A: monitor at home; B: see a doctor in a few weeks; C: see a doctor in 24-48 hours; D: go to emergency). Half the cases carry dual labels gold-standards, e.g., *C/D* at 24/60, and either label is treated as an acceptable match in scoring (full distribution in Appendix A).

3.2 Models and SAEs

Both SAE pipelines decompose residual streams into sparse interpretable features (Bricken et al., 2023; Cunningham et al., 2023; Templeton et al., 2024): Gemma Scope 2 uses JumpReLU (Rajamanoharan et al., 2025; Lieberum et al., 2024), while Qwen-Scope uses TopK with $k=100$ (Makhzani and Frey, 2013; Gao et al., 2024; Qwen Team, 2026). We use Gemma 3 4B IT (34 layers, $d_{\text{model}} = 2560$) and Gemma 3 12B IT (48 layers, $d_{\text{model}} = 3584$) with Gemma Scope 2 SAEs ($d_{\text{SAE}} = 16,384$, $\sim 14\%$ reconstruction error), and Qwen3-8B (36 layers, $d_{\text{model}} = 4096$) with Qwen-Scope SAEs ($d_{\text{SAE}} = 65,536$, $\sim 34\%$ reconstruction error at L31). For Gemma we sweep four matched-depth layers at $\approx 27\%, 50\%, 65\%, 85\%$ of total depth: in 4B layers 9, 17, 22, 29 and in 12B layers 12, 24, 31, 41. For Qwen we use layer 31 at $\approx 86\%$ relative depth, selected by reconstruction error from a four-layer pilot sweep (Appendix D).

3.3 Behavioral test

For each case we generate output via greedy decoding (Holtzman et al., 2019). SL and NL answers are extracted via regex. NF and SF free-text are scored by gpt-5.2-thinking-high and claude-sonnet-4.6 LLM judges, adjudicating against the gold label on the A–D scale, with acceptable matches on dual-labeled cases. Letter-extraction (SL, NL) and LLM-judge (SF, NF) pipelines therefore score slightly different artifacts (the emitted letter vs. an interpreted commitment from free text); we treat this as part of the format contrast, not a noise source to be removed. We report per-condition accuracy, and inter-rater agreement and Cohen’s κ as a calibration signal. A clinician-adjudicated subset (Section 3.8, Appendix I) provides external calibration of the LLM judges against clinical judgment on a stratified 16-case sample.

To disambiguate whether multiple-choice accuracy depends on letter position or letter content, we run an exhaustive shuffle of the letter→content mapping in NL. For each of the 60 NL prompts,

we generate all 23 non-identity permutations of the assignment $\{A, B, C, D\}$, keeping option texts verbatim but rewriting the letter labels (e.g., “see a doctor in 24–48 hours” may sit under any letter). We re-run multiple-choice generation on each shuffled prompt under greedy decoding ($60 \times 23 = 1380$ NL passes per model). For each shuffle we record both the picked letter and the picked content. Position bias predicts a constant picked letter across shuffles; a content prior predicts constant picked content. Case-clustered 95% CIs are bootstrapped over cases (2,000 resamples; full protocol in Appendix U).

3.4 Mechanistic invariance test

For each (model, layer, case, condition) we encode the residual stream through the SAE and **max-pool feature activations** over user-content tokens: each feature contributes its peak activation on any token (pooling conventions in Appendix M). To avoid mean-pool dilution we use Max-pooling for Qwen-Scope’s $k=100$ TopK sparsity; Gemma aggregation checks are in Appendix L. We compare two feature subsets \mathcal{F} : the 3 contrastively-identified medical features per layer (Section 3.9) and a magnitude-matched *random* control of 30 features drawn per layer from the non-medical feature pool (size 500–2,200; full protocol in Appendix N). For each case and each subset \mathcal{F} , we summarize NL-NF invariance by two statistics. The first is the symmetric mean absolute percentage error (sMAPE, Makridakis, 1993) in its standard form, applied here over the features in \mathcal{F} :

$$\text{sMAPE}_{\mathcal{F}} = \frac{1}{|\mathcal{F}|} \sum_{f \in \mathcal{F}} \frac{|a_{\text{NL}}^f - a_{\text{NF}}^f|}{(|a_{\text{NL}}^f| + |a_{\text{NF}}^f|)/2},$$

where a_{NL}^f and a_{NF}^f are feature f ’s max-pooled activations in the NL and NF conditions; lower = more invariant. In implementation we floor the denominator at $\varepsilon = 10^{-8}$ to prevent division by zero when both activations are exactly zero; this affects only inactive features and leaves active-feature scores unchanged. The second statistic is cosine similarity between the NL and NF feature-subset activation vectors (higher = more invariant).

We stratify case-level results by joint NL-NF correctness into five strata: both-right, both-wrong, NF-only-right (NL wrong, NF correct), NL-only-right (the inverse), and judges-disagree (withheld from headline tables). For each (layer, stratum) we

report bootstrap 95% CIs on the per-case medical-random Δ for both sMAPE and cosine. The bootstrap resamples the n cases in the stratum with replacement, computes the resample mean, repeats this 2,000 times, and takes the 2.5th and 97.5th percentiles.

Analyzed late layer. We report results in body at a single late layer per model (4B L29, 12B L31, Qwen L31), the deepest layer in the sweep of Section 3.2; the full per-layer / per-stratum tables are in Appendix K. The body layer is chosen for two reasons that the sweep itself documents. First, the direction analysis (Section 3.7, Appendix K) shows that late-layer encoder columns are where the residual (NL–NF) direction projects onto non-medical scaffold features: the layer at which the question “are medical features format-invariant while the format direction lives elsewhere?” is most cleanly testable. Second, at Gemma 12B the medical–random difference reverses sign between shallow/mid layers (L12, L24) and late layers (L31, L41); the late layers are the regime where the invariance pattern is stable, and we report the shallow/mid behavior separately in Appendix K.

3.5 Decision-token analyses

We target the hidden state at the NL pre-generation token (the last user-message token, whose hidden state drives the first generated letter) with one primary analysis and two SAE-pool corroborations.

On Gemma 3 12B IT (the only open-weight NLA checkpoint we have access to (Fraser-Taliente et al., 2026)), at layer 32, we capture residual-stream activations at seven token positions (CONTENT, DECISION, and four letter_A/B/C/D; full positions in Appendix Q), pass them through the released NLA, and have the two LLM judges classify each generated description on two axes: (MEDICAL and SCAFFOLD, each PRIMARY/PARTIAL/NO).

Two complementary analyses on the SAE feature pool at the same decision token — decision-token logit attribution via $\text{contrib}(f, \ell) = a_f W_{\text{dec}}[:, f]^T W_U[:, t_\ell]$, and top-20-by-activation feature characterization with Jaccard overlap and scaffold-peak diagnostic corroborate the NLA result quantitatively. Full methodology, feature-category definitions, and the linear-projection caveats are in Appendices V and W.

3.6 Predicting behavioral instability from source-format representation

To test whether the format-induced representational shift can predict behavioral flipping, we train linear probes (L2-regularized logistic regressionsolver) on Gemma 3 4B IT last-token hidden states ($d=2,560$) at layers {9, 17, 19, 22, 25, 27, 29, 31, 33, 34}. For each format transition (e.g., NL→SL), the binary target is whether correctness flips. The last-token embedding is the only representation that has attended to the full input under the model’s causal mask, making it the most direct readout of pre-generation state. Under *Constraint-First* (CF) condition, we move the formatting instructions to the start of the prompt to disentangle if the representational shift may be a positional artifact. Training uses leave-one-out cross-validation with balanced class weighting.

We report ROC-AUC and PR-AUC with p -values from 1,000-iteration permutation tests per layer and transition. ROC-AUC reflects global ranking ability across the sample, while PR-AUC bounded by the class prevalence rate provides a more conservative estimate of discriminative power for the minority class.

3.7 Direction-of-format-effect test

To localize the NL-NF residual-stream direction in the SAE basis, we average per-case residual differences into Δr and rank SAE encoder columns by their absolute cosine alignment with this direction, $|\cos(\Delta r, W_{\text{enc}}[:, f])|$, where $W_{\text{enc}}[:, f]$ is the encoder column for feature f (i.e. the direction the SAE uses to detect feature f in the residual stream). We then report medical-feature percentile ranks in this ordering (0% is top-aligned). NL is longer than NF by the appended multiple-choice scaffold (50–60 tokens), so different aggregation choices conflate the format direction with token counts. We therefore run three aggregations to separate scaffold length from format: **full mean-pool** averages per-token residuals over each condition’s full content range (so NL includes the scaffold); **length-controlled mean-pool** averages only over the byte-identical clinical-prefix tokens that both conditions share (no scaffold contribution); **max-pool** takes each feature’s peak activation over content tokens and is therefore length-invariant.

3.8 Deferral adjudication

The above 4-way scoring forces judges to convert each free-text response to one letter. Inspection of 12B NF outputs revealed *deferrals*: that condition on missing clinical information, (e.g., “ER if BP>180/120; same-day clinic if 140–180; review within two weeks otherwise”). We re-adjudicate every NF response under $\{A, B, C, D, DEFERRED\}$ with the same two LLM judges (full protocol, label definition, and stratum-mapping rules in Appendix H). To check if the deferrals are clinically appropriate, a clinician (anonymized), blinded to LLM-judge labels and model identity, adjudicated a 16-case sample. The sample is stratified across four cells of 4 cases each: three at 12B (12B-both-deferred, 12B-clear-correct, 12B-clear-incorrect, covering the deferral phenomenon at the scale where it occurs) plus one cross-scale cell at 4B (4B-format-flipped, NL letter wrong but NF judged correct, our gap-driver stratum). Per-case appropriateness judgments and the clinician’s deferral rate are reported in Appendix I.

3.9 Medical-feature identification

For Gemma 3 4B IT we use 3 medical features per analyzed layer, identified in (Fraile Navarro, 2026) via a 6-condition cross-lingual contrastive over MMLU question stems (three languages \times medical/non-medical; full protocol in Appendix B). For Gemma 3 12B IT and Qwen3-8B we instead run an English-only medical-vs-non-medical contrastive at each analyzed layer, using the 60 NF prompts as the medical set and 30 patient-voiced non-medical prompts as control (Appendix C). Following the mean-conditional-activation contrast (Bricken et al., 2023; Templeton et al., 2024), features are scored by $\mathbb{E}_{\text{med}}[\max_t a_f] - \mathbb{E}_{\text{non}}[\max_t a_f]$, where $\mathbb{E}[\cdot]$ is the empirical mean of feature f ’s per-prompt peak activation over the medical/non-medical prompt set. Features are then filtered for selectivity ($\geq 70\%$ medical and $\leq 10\%$ non-medical firing above threshold 1.0) and the top-3 are retained. A K -sweep confirms stability across $K \in \{3, 5, 10, 20\}$ (Appendix G); within-corpus feature identification at 12B and Qwen is scoped in Section 6.

4 Results

4.1 Behavioral differences

We measure condition-level accuracy on all 60 cases in the corpus (Section 3.1), Table 1. NF and

SF responses are scored by two LLM judges under the four-letter adjudication prompt of Section 3.3.

Condition	4B	12B	Qwen
SL (structured + multiple-choice)	58.3%	81.7%	75.0%
SF (structured + free-text)	63.3%	73.3%	70.0%
NL (natural + multiple-choice)	55.0%	81.7%	75.0%
NF (natural + free-text)	71.7%	71.7%	68.3%
Natural input: NF–NL	+16.7	−10.0	−6.7
Structured input: SF–SL	+5.0	−8.3	−5.0

Table 1: Condition-level accuracy on the 60 cases, completing the 2×2 factorial design.

Cross-input robustness. The difference between the free-text and multiple-choice output is positive at 4B (+16.7/+5.0pp for natural/structured) input, and negative at 12B (−10.0/−8.3pp) and Qwen (−6.7 / −5.0pp). Paired McNemar tests on the NF–NL gap give $p=0.031$ at both Gemma scales and $p=0.45$ at Qwen (n.s. at $n=60$). The same test on the SF–SL gap is in the same direction at every model but does not reach significance at $n=60$ ($p=0.63$ at 4B, $p=0.18$ at 12B, $p=0.58$ at Qwen). Free-text scores are scored as both-judge agreement under 4-way adjudication; per-judge breakdown and inter-rater κ in Appendix H. The SF–SL row therefore points in the same direction as the NF–NL row at every scale, but with smaller magnitude (lgap| 5–8pp vs. 7–17pp for NF–NL) and is statistically underpowered at $n=60$. The cross-input-style claim is most cleanly supported at 4B, where NF–NL = +16.7pp ($p=0.031$); the structured-input row is suggestive evidence that the same output-side mechanism applies across input style, not independent statistical confirmation. The structured-vs-natural input contrast (SX–NX) is near-zero in every cell except 4B SF<NF (−8.4pp), which traces to deferral-priming under structured input in the smaller model (Section 4.2).

NL–NF performance details. We consider the more ecologically valid free-text input/output. At Gemma 4B, NF exceeds NL by +17–22pp depending on the NF judge (+17pp under the conservative both-judges rule), replicating the constrained-output penalty of (Fraile Navarro et al., 2026); the 5-way refinement finds no unanimous deferrals. At Gemma 12B, NF sits 10pp, and at Qwen 6.7pp below NL. The 4B free-text gain is concentrated where adjacent dispositions compete: gold C (NL 10% \rightarrow NF 80%, +70pp) and gold C/D (+21pp), spanning the Intermediate and High acuity tiers.

The 12B pattern is inverse, with NF underperforming most on gold *D* (−25pp) and gold *C* (−20pp) (Table 6). At Qwen, NF is weakest on the low-acuity gold *A* (−24pp; Table 7), consistent with the 12B patterns. Per-acuity breakdowns for 4B and 12B in Appendix E.

Triage error direction. The direction of misclassifications matters clinically since under-triage (lower than gold predicted acuity) is a dangerous direction. Multiple-choice NL errors are skewed toward under-triage at 4B (20 NL errors are under- and 7 over-triage) and Qwen (12 under, 3 over), whereas NF errors are approximately balanced at all models (under/over: 5/8 at 4B, 8/9 at 12B, 8/6 at Qwen). A clinically concerning corner case at 4B: on the $n=4$ singleton gold-*D* cases, 4B’s NL never predicts *D* and NF only. Full breakdown in Appendix E.

4.2 Decomposing accuracy gap

The gaps in Table 1 have two plausible explanations: **single-acuity-step miscalibration** between formats (dominates) or **deferral** (benchmark-adequacy concern). Per-case decomposition for all models in Appendix T; Table 2 summarises.

Model	NF_OR	NL_OR	DEF	in gap	Adj.
4B	14	1	0	0	14/14 + 1/1
12B	0	6	4	0	5/6
Qwen	6	8	2	0–2	1/6 + 8/8

Table 2: Decomposition of the NL-NF accuracy gap. $NF_OR / NL_OR = NF\text{-only-right} / NL\text{-only-right}$ counts; DEF = unanimous DEFERRED cases under 5-way scoring; *in gap* = contribution to the 4-way-scored gap (deferrals flattening to gold-compatible letters count as correct, 0; Qwen’s two deferrals are judges-disagree, 0–2); Adj. = fraction of gap-driving cases that are single-acuity-step miscalibrations.

Adjacent miscalibration drives the gap. At Gemma 4B, the 14 gap-driving cases share a single pattern: NL picks B, gold is C, and NF picks C in 13/14. In the multiple-choice mode, 4B systematically commits to B on cases where the gold disposition is C, while the same model under free-text reaches the correct answer. Exhaustive option-order shuffles (Section 3.3, Appendix U) rule out an alternative explanation that 4B is positionally biased toward *B*: across all models the picked letter is at or below chance under shuffles (case-clustered 95% CI excludes 25% at 4B and

12B; contains it at Qwen), while picked *content* stays far above chance (64.%, 80.3%, 82.6% at 4B, 12B, Qwen). At 4B specifically, randomizing the letter-to-content assignment raises NL’s accuracy from 55.0% to 69.8%, statistically indistinguishable from NF’s 71.7%. Thus, 4B’s gap comes from the original benchmark answer-key layout interacting with the model’s content prior, not from positional bias. The two factors are established independently in the same experiment, content prior by the above-chance picked-content rate, position bias ruled out by the at-chance picked-letter rate, and their interaction is probed by the layout shuffle, which raises 4B accuracy to NF level while leaving 12B and Qwen 8B mostly unchanged. At 12B and Qwen, the canonical mapping is approximately neutral (−2.8 and −2.2pp under shuffle), but a residual NF-side penalty remains 4.6 and 7.1pp. At scale, free-text mode contributes its own adjacent-miscalibration penalty independently of the answer-key mapping.

DEFERRED answers explain partially accuracy drop. Under the 5-way label space of Section 3.8, NF gives a conditional answer instead of committing to a letter in 4 cases at 12B, 2 at Qwen, and none at 4B. When these are re-scored under the original 4-letter space, all 12B deferrals flatten to a gold-compatible letter and count as correct, not contributing to the 12B gap; the Qwen deferrals receive split judgments from the two LLM judges (judges-disagree) and contribute partially. A clinician judged 3 of the 12B deferrals clinically appropriate (Appendix I). The structured-input SF condition shows the inverse profile (4 unanimous deferrals at 4B, none at Qwen), suggesting that structured-format inputs prime conditional responses in the smaller model, a pattern worth following up in the future. Answer deferral is therefore a label-space concern: the 4-letter benchmark cannot express conditional triage boundaries, but it is not the driver of the observed accuracy inversion.

4.3 Mechanistic invariance: magnitude

We test whether medical SAE features show greater format-invariance than random features (Section 3.9) under both summary metrics defined in Section 3.4. We report the late layer per model (4B L29, 12B L31, Qwen L31; rationale and per-layer behavior in Section 3.4 and Appendix K).

Medical features. $\Delta sMAPE < 0$ and $\Delta \cos > 0$ both indicate medical features are more format-

Model / Layer	Stratum	n	Δ sMAPE	Δ cos
4B L29	both-right	29	-0.275*	+0.054*
	both-wrong	12	-0.336*	+0.060*
	NF_OR	14	-0.338*	+0.049*
12B L31	both-right	43	-0.222*	+0.093*
	both-wrong	11	-0.232*	+0.094*
	NL_OR	6	-0.262*	+0.093*
Qwen L31	all	60	-0.070*	+0.004*

Table 3: Late-layer per-stratum medical-random feature difference. * marks cells significant at $p < 0.05$ (bootstrap 95% CI excludes zero, 2,000 resamples). At 12B the NF-only-right cell is empty; the 6-case NL-only-right stratum substitutes (the gap-driver at this scale; Section 4.2). Per-layer / per-stratum tables in Appendix K; sanity checks in Appendices R and S.

invariant than the magnitude-matched random control. At every cell of 4B L29 and 12B L31 the difference is significant on both metrics (bootstrap 95% CIs non-zero). Qwen L31 reproduces the direction at smaller effect size, consistent with Qwen-Scope’s higher reconstruction error (Section 3.2).

A natural concern is that NL and NF share the same clinical vignette verbatim, and tokens inside that shared block can only attend leftward, so their hidden states are identical across formats. The invariance we report is different. Under max-pool, the medical features’ peak activations actually *lie inside* the shared clinical vignette in 98.3–100% of (case, feature) combinations across all three models, whereas the magnitude-matched random features peak on the NL-only scaffold tokens. The medical features are tracking clinical content; the random pool is not.

To rule out the mechanical reading we conduct additional checks. *First*, a vignette-only token mask restricts both pools to tokens inside the shared clinical block. sMAPE drops to 0.002-0.006 for medical and random features alike (Appendix R), confirming that the format contrast lives outside the vignette and the observed medical-random gap would not arise from prefix-attention alone. *Second*, 1,000 magnitude-matched random resamples preserve the medical-random gap at $p < 0.001$ at every model (Appendix S). *Third*, restricting the random pool to features that fire on $\geq 25\%$ of the NL/NF prompts, so the comparison is against content-firing features, leaves every stratum’s 95% CI non-zero on both metrics, with modest magnitude changes relative to the unrestricted control (per-stratum results in Appendix K, where the Gemma 12B shallow/mid sign inversion at

L12/L24 is shown). Taken together, medical-domain content is preserved on the clinical narrative across formats; this is a representational claim about the clinical content, not about whether the model encodes the correct triage disposition.

Direction of the residual difference. Where does the format direction live in the SAE? We project the case-averaged NF-NL residual onto SAE encoder columns under the length-invariant max-pool aggregation of Section 3.7 and rank features by absolute alignment. Across all three models, the medical features land at mid-rank percentiles (median 47%, IQR 33–68%, with 11/12 Gemma layer-feature combinations outside the top decile). The format direction therefore lives primarily in *non-medical* features. The pattern is consistent across the three aggregations (full mean-pool, length-controlled mean-pool, and max-pool; Section 3.7), and top-token inspection of the most-aligned 4B L29 features shows them firing on NL-only answer-key scaffold tokens. Full ranks and the per-aggregation comparison are in Appendices K and P.

Repeating the medical-random invariance test on the structured-input SL-SF pair at the same layers yields paired Δ sMAPE values of -0.081 at 4B L29, -0.062 at 12B L31, and -0.150 at Qwen L31, all with 95% CI strictly non-zero. The format-effect localization therefore generalizes from the naturalistic free-text to the structured format. Full table in Appendix X.

4.4 Decision-token mode shift

So far the analyses have averaged or max-pooled over the clinical content. We now turn to the NL pre-generation token, where the multiple-choice letter is decided. Our primary tool here is the Natural Language Autoencoder (NLA) Fraser-Taliente et al. (2026), an unsupervised method *independent of SAE* that produces natural-language descriptions of residual-stream activations. We capture L32 activations of Gemma 3 12B IT at seven token positions under NL and NF (Section 3.5, Appendix Q) and the LLM judges classify each description’s MEDICAL and SCAFFOLD grade, with three classes each: PRIMARY – description’s main subject, PARTIAL – secondary mention, or NO – or absent. The judges agree 96.7% and 96.2% of time on the respective axes (Table 4).

Representation flips at the decision token. At NF_content and NL_content the residual reads as

Position	MEDICAL ($n=60$)			SCAFFOLD ($n=60$)		
	PRIM	PART	NO	PRIM	PART	NO
NF_content	60	0	0	0	8	52
NL_content	60	0	0	0	7	53
NL_decision	0	60	0	60	0	0
NL_letter_A	0	60	0	60	0	0
NL_letter_B	0	8	52	60	0	0
NL_letter_C	0	57	3	60	0	0
NL_letter_D	0	60	0	60	0	0

Table 4: LLM-judge classifications of NLA descriptions across 7 token positions, with headline cells shaded. NF_content/NL_content: clinical content is the MED-PRIMARY frame under both formats. NL_decision: the content frame is demoted to MED-PARTIAL and a SCA-PRIMARY multiple-choice-scaffold encoding takes over.

MED-PRIMARY in all cases under both formats: the NLA describes clinical content as the main subject of the hidden state. At NL_decision one token later, the frame flips: no MED-PRIMARY, 60 MED-PARTIAL, 60 SCA-PRIMARY (Table 4). The multiple-choice scaffold does not strip clinical content, but *demotes* that content from the representation’s main subject to a secondary mention while a multiple-choice-scaffold concept becomes the primary subject. Representative NLA outputs are in Appendix Q.

SAE-pool corroboration. Two diagnostics on the SAE feature pool confirm the NLA reading. *First*, the three contrastively-identified medical features used in Section 4.3 have no activation at the NL pre-generation token in 60 cases at every model, and contribute 0% of the absolute linear effect on the A/B/C/D logits via the per-feature unembedding projection (Appendix V). *Second*, top-20 active features at the NL and NF decision tokens are essentially disjoint at Gemma and share 32% at Qwen. Across all models, 87-95% of features unique to NL’s top-20 peak on scaffold tokens outside the shared clinical vignette and no identified medical features appear in either top-20 at any model (Appendix W). These results concur with NLA: medical-content detectors fire on the clinical narrative during reading, then go silent before the letter is selected, while scaffold features drive the letter logits. Full numerical breakdown including scaffold-other split in Appendices V and W.

4.5 Source-format representation predicts behavioral flipping

If the decision-token mode shift (Section 4.4) drives the behavioral gap, the source-format hidden

state alone may predict which cases flip under a format change. We test this on Gemma 3 4B IT.

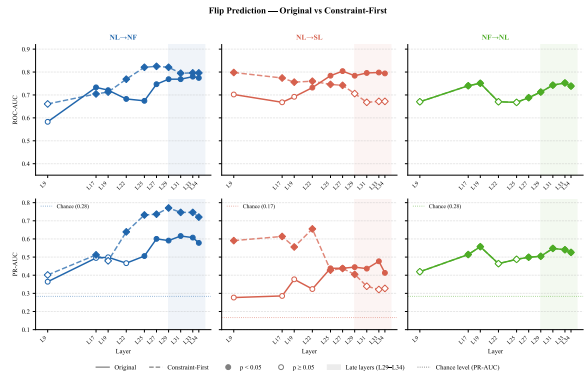


Figure 1: Linear probe AUC and PR-AUC performance with p-values for NL \rightarrow NF, NL \rightarrow SL, NF \rightarrow NL.

Predictive signal concentrates in the deep layers of the network (L29-L34). For NL \rightarrow NF, we obtain AUC=0.769 – 0.780, $p = 0.004$ and PR-AUC=0.591 – 0.616 vs baseline 0.283; for NL \rightarrow SL – AUC=0.784 – 0.804, $p = 0.010$ and PR-AUC=0.413 – 0.477 vs baseline 0.167; and for NF \rightarrow NL – AUC=0.713 – 0.752, $p = 0.009$ – 0.023 (see Figure 1). Among the four source prompt formats, NL-sourced last-token embeddings produce the most consistent predictive signal across target directions at late layers. All the results are in Appendix Y.

Moving the formatting instruction to the beginning of the prompt in constraint-first ablation selectively modifies the late-layer predictive signal for the two NL-sourced transitions. For NL_CF \rightarrow NF, AUC at the same levels increases by 0.016 – 0.052 ($p = 0.001$ – 0.003), while for NL_CF \rightarrow SL it degrades by 0.078 – 0.128 and loses significance. NF-sourced directions were identical across both runs since NF does not have output constraints.

5 Conclusion

Across three instruction-tuned consumer LLMs from two families, four converging observations support an output-mapping reading of the apparent multiple-choice triage failures. *First*, the same medical features fire on the shared clinical narrative under both formats and peak inside the vignette in 98–100% of (case, feature) combinations. *Second*, at the multiple-choice decision token they go silent and scaffold-encoding features take over, with NLA verbalization and SAE-pool diagnostics agreeing on this flip. *Third*, the multiple-choice accuracy

penalty inverts with scale identically under natural-language and structured input, so the effect originates on the output side rather than in phrasing. *Fourth*, the measured NL-NF accuracy gap is dominated by single-acuity-step miscalibration, not by deferral; the parallel SL-SF gap shows a comparable profile (Section 4.2). A per-case decomposition on SL-SF is outside this paper’s scope.

6 Limitations

Coverage and sample size. We study 60 patient-voiced clinical-triage vignettes per model across three instruction-tuned consumer LLMs from two families, with greedy decoding only. Small behavioral strata and the one-layer Qwen analysis limit generalization beyond Gemma and Qwen. The Qwen behavioral gap is not significant at $n=60$ (McNemar $p=0.45$); the Qwen mechanistic findings nonetheless reproduce the Gemma direction at smaller effect size, consistent with Qwen-Scope’s higher reconstruction error on the residual stream.

Judging and clinical calibration. NF scoring relies on two LLM judges under an A–D label space that flattens some tiered DEFERRED responses. The clinician subset is enriched and small ($n=16$, Appendix I); it calibrates label face validity, not clinical deferral prevalence or deployment safety.

Mechanistic-method scope. We use max/mean pooling and encoder-direction projection rather than richer aggregations or a full multi-feature intervention sweep. Qwen-Scope’s $\sim 34\%$ L31 reconstruction error raises the Qwen noise floor. Feature identification at 12B and Qwen reuses the 60 NF prompts with a 30-prompt non-medical contrastive; a held-out contrastive split would tighten inference. The random baseline is magnitude-matched and resampled (Appendix S) to avoid zero-firing denominator artifacts.

Claim scope. The SAE features are medical-vs-non-medical detectors, not acuity probes: we claim medical-domain content is preserved on the clinical narrative, not that correct triage disposition is encoded. Shared-prefix pooling contains causal-masking-trivial invariance, which we isolate with token masks and content-anchored peaks (Appendix R). NLA evidence is limited to Gemma 3 12B IT, the released checkpoint available for this analysis (Fraser-Taliente et al., 2026). Causal interventions on the format-direction features at 4B L29 (discrete SAE-feature ablation and continuous

ActAdd steering; Appendix O) change only 0–2 of 60 NL predictions, consistent with the multi-intervention nulls of (Basu et al., 2026); we therefore treat the SAE features as *readout probes* of medical-domain content rather than as causal handles or clinical monitors.

Decision-token feature sets do not overlap across formats. At the NL pre-generation token, the top-20 most active features are nearly disjoint between NL and NF at both Gemma scales (Jaccard ≈ 0 ; 0.32 at Qwen), and *none* of the contrastively-identified medical features appear in either set (Appendix W). The scaffold-firing features that dominate the NL letter logits are therefore not reweightings of the same feature pool active under NF; they are a different set of features entirely. We do not yet know what these features encode beyond “peak on answer-key scaffold tokens,” nor whether they reflect learned answer-key templates from pretraining/instruction tuning or something more specific to the clinical-triage register; characterising them is left to future work.

Clinical claim scope. Lower forced-letter under-triage in some comparisons is not a safety endorsement of NF. Deferrals, hedging, and emergency-tier misses persist; our claim concerns the adequacy of forced-letter evaluation as a competence readout, not the deployment-readiness of free-text outputs. Late-layer SAE features are a *candidate readout* of medical-domain representation, not a validated clinical monitor: deployment would require held-out calibration, robustness checks, correlation with under-triage risk, and prospective validation. The intervention nulls here and in (Basu et al., 2026) also argue against single-layer SAE control as a correction method on this task.

7 Use of AI assistants

We used AI assistants: Claude Code (Anthropic, an agentic command-line coding tool) and Claude Opus 4.7 (Anthropic); at three stages of this work: (i) implementing analysis code (SAE encoding, bootstrap and case-clustered CI routines, option-order shuffles, decision-token logit attribution, the NLA judge-classification pipeline, and the linear-probe training); (ii) executing experiments under human supervision (model loading, hooked forward passes, activation extraction, judge-call orchestration), with authors verifying outputs against unit tests and independent reproductions where ap-

plicable; and (iii) paper preparation (LaTeX editing, prose tightening on the basis of co-author and reviewer comments, bibliography reconciliation). Research design, hypotheses, method and model selection, interpretation of results, abstract drafting, and final claims were authored and verified by the human authors; AI assistants did not generate research ideas, choose what to evaluate, decide which results to report, or write the core narrative or abstract. The authors take full responsibility for all numerical results, code, and claims.

References

- Sanjay Basu, Sadiq Y. Patel, Parth Sheth, Bhairavi Muralidharan, Namrata Elamaram, Aakriti Kinra, John Morgan, and Rajaie Batniji. 2026. [Interpretability without actionability: mechanistic methods cannot correct language model errors despite near-perfect internal representations](https://arxiv.org/abs/2603.18353). *arXiv preprint arXiv:2603.18353*. Submitted 2026-03-18 (verified 2026-05-11).
- Trenton Bricken, Adly Templeton, Joshua Batson, Brian Chen, Adam Jermy, Tom Conerly, Nick Turner, Cem Anil, Carson Denison, Amanda Askell, Robert Lasenby, Yifan Wu, Shauna Kravec, Nicholas Schiefer, Tim Maxwell, Nicholas Joseph, Zac Hatfield-Dodds, Alex Tamkin, Karina Nguyen, and 6 others. 2023. [Towards monosemanticity: Decomposing language models with dictionary learning](https://transformer-circuits.pub/2023/monosemantic-features). <https://transformer-circuits.pub/2023/monosemantic-features>.
- Collin Burns, Haotian Ye, Dan Klein, and Jacob Steinhardt. 2023. [Discovering latent knowledge in language models without supervision](https://arxiv.org/abs/2309.08600). *International Conference on Learning Representations*.
- Hoagy Cunningham, Aidan Ewart, Logan Riggs, Robert Huben, and Lee Sharkey. 2023. [Sparse autoencoders find highly interpretable features in language models](https://arxiv.org/abs/2309.08600). *arXiv preprint arXiv:2309.08600*.
- David Fraile Navarro. 2026. [Sae-guided cross-lingual knowledge transfer in llms: A null result with preserved findings](https://github.com/dafraile/SAE_mad). https://github.com/dafraile/SAE_mad.
- David Fraile Navarro, Farah Magrabi, and Enrico Coiera. 2026. [Evaluation format, not model capability, drives triage failure in the assessment of consumer health AI](https://arxiv.org/abs/2603.11413). *arXiv preprint arXiv:2603.11413*. Submitted 2026-03-12, v3 revised 2026-03-26 (verified 2026-05-11).
- Kit Fraser-Taliente, Subhash Kantamneni, Euan Ong, Dan Mossing, Christina Lu, Paul C. Bogdan, Emmanuel Ameisen, James Chen, Dzmitry Kishylau, Adam Pearce, Julius Tarnig, Alex Wu, Jeff Wu, Yang Zhang, Daniel M. Ziegler, Evan Hubinger, Joshua Batson, Jack Lindsey, Samuel Zimmerman, and Samuel Marks. 2026. [Natural language autoencoders produce unsupervised explanations of LLM activations](https://transformer-circuits.pub/2026/nla/index.html). <https://transformer-circuits.pub/2026/nla/index.html>. Anthropic; published 2026-05-07. First three authors contributed equally (listed alphabetically among them).
- Leo Gao, Tom Dupré la Tour, Henk Tillman, Gabriel Goh, Rajan Troll, Alec Radford, Ilya Sutskever, Jan Leike, and Jeffrey Wu. 2024. [Scaling and evaluating sparse autoencoders](https://arxiv.org/abs/2406.04093). *arXiv preprint arXiv:2406.04093*.
- Ari Holtzman, Jan Buys, Li Du, Maxwell Forbes, and Yejin Choi. 2019. [The curious case of neural text degeneration](https://arxiv.org/abs/1904.09751). *arXiv preprint arXiv:1904.09751*.
- Saurav Kadavath, Tom Conerly, Amanda Askell, Tom Henighan, Dawn Drain, Ethan Perez, Nicholas Schiefer, Zac Hatfield-Dodds, Nova DasSarma, Eli Tran-Johnson, Scott Johnston, Sheer El-Showk, Andy Jones, Nelson Elhage, Tristan Hume, Anna Chen, Yuntao Bai, Sam Bowman, Stanislav Fort, and 17 others. 2022. [Language models \(mostly\) know what they know](https://arxiv.org/abs/2207.05221). *arXiv preprint arXiv:2207.05221*.
- Tom Lieberum, Senthoooran Rajamanoharan, Arthur Conmy, Lewis Smith, Nicolas Sonnerat, Vikrant Varma, János Kramár, Anca Dragan, Rohin Shah, and Neel Nanda. 2024. [Gemma scope: Open sparse autoencoders everywhere all at once on gemma 2](https://arxiv.org/abs/2405.08366). In *Proceedings of the 7th BlackboxNLP Workshop: Analyzing and Interpreting Neural Networks for NLP*, pages 217–232.
- Aleksandar Makelov, Georg Lange, and Neel Nanda. 2024. [Towards principled evaluations of sparse autoencoders for interpretability and control](https://arxiv.org/abs/2405.08366). *arXiv preprint arXiv:2405.08366*. Verify before submission.
- Alireza Makhzani and Brendan Frey. 2013. [k-sparse autoencoders](https://arxiv.org/abs/1312.5663). *arXiv preprint arXiv:1312.5663*.
- Spyros Makridakis. 1993. [Accuracy measures: theoretical and practical concerns](https://arxiv.org/abs/1904.09751). *International Journal of Forecasting*, 9(4):527–529.
- Samuel Marks, Can Rager, Eric J. Michaud, Yonatan Belinkov, David Bau, and Aaron Mueller. 2024. [Sparse feature circuits: Discovering and editing interpretable causal graphs in language models](https://arxiv.org/abs/2403.19647). *arXiv preprint arXiv:2403.19647*.
- Pouya Pezeshkpour and Estevam Hruschka. 2024. [Large language models sensitivity to the order of options in multiple-choice questions](https://arxiv.org/abs/2405.08366). In *Findings of the Association for Computational Linguistics: NAACL 2024*.
- Qwen Team. 2026. [Qwen-scope: Decoding intelligence, unleashing potential](https://qwen.ai/blog?id=qwen-scope). <https://qwen.ai/blog?id=qwen-scope>. Accessed 2026-05-02.

- Senthooran Rajamanoharan, Tom Lieberum, Nicolas Sonnerat, Arthur Conmy, Vikrant Varma, János Kramár, and Neel Nanda. 2025. [Jumping ahead: Improving reconstruction fidelity with jumprelu sparse autoencoders](#). In *International Conference on Learning Representations*.
- Ashwin Ramaswamy, Alvira Tyagi, Hannah Hugo, Joy Jiang, Pushkala Jayaraman, Mateen Jangda, Alexis E. Te, Steven A. Kaplan, Joshua Lampert, Robert Freeman, Nicholas Gavin, Ashutosh K. Tewari, Ankit Sakhuja, Bilal Naved, Alexander W. Charney, Mahmud Omar, Michael A. Gorin, Eyal Klang, and Girish N. Nadkarni. 2026. [Chatgpt health performance in a structured test of triage recommendations](#). *Nature Medicine*. DOI resolves on nature.com (verified 2026-05-11); add volume/issue/pages for camera-ready.
- Melanie Sclar, Yejin Choi, Yulia Tsvetkov, and Alane Suhr. 2024. [Quantifying language models’ sensitivity to spurious features in prompt design or: How i learned to start worrying about prompt formatting](#). In *International Conference on Learning Representations*.
- Karan Singhal, Shekoofeh Azizi, Tao Tu, S. Sara Mahdavi, Jason Wei, Hyung Won Chung, Nathan Scales, Ajay Tanwani, Heather Cole-Lewis, Stephen Pfohl, Perry Payne, Martin Seneviratne, Paul Gamble, Chris Kelly, Abdelrahman Babiker, Nathanael Schärli, Aakanksha Chowdhery, Philip Mansfield, Dina Demner-Fushman, and 8 others. 2023. [Large language models encode clinical knowledge](#). *Nature*, 620(7974):172–180.
- Karan Singhal, Tao Tu, Juraj Gottweis, Rory Sayres, Ellery Wulczyn, Le Hou, Kevin Clark, Stephen R. Pfohl, Heather Cole-Lewis, Darlene Neal, and 1 others. 2025. [Toward expert-level medical question answering with large language models](#). *Nature Medicine*. Med-PaLM 2; verify final citation details before submission.
- Adly Templeton, Tom Conerly, Jonathan Marcus, Jack Lindsey, Trenton Bricken, Brian Chen, Adam Pearce, Craig Citro, Emmanuel Ameisen, Andy Jones, Hoagy Cunningham, Nicholas L. Turner, Callum McDougall, Monte MacDiarmid, C. Daniel Freeman, Theodore R. Sumers, Edward Rees, Joshua Batson, Adam Jermyn, and 2 others. 2024. [Scaling monosemanticity: Extracting interpretable features from claude 3 sonnet](#). <https://transformer-circuits.pub/2024/scaling-monosemanticity/>.
- Alexander Matt Turner, Lisa Thiergart, Gavin Leech, David Udell, Juan J. Vazquez, Ulisse Mini, and Monte MacDiarmid. 2023. [Steering language models with activation engineering](#). *arXiv preprint arXiv:2308.10248*.
- Miles Turpin, Julian Michael, Ethan Perez, and Samuel R. Bowman. 2023. [Language models don’t always say what they think: Unfaithful explanations in chain-of-thought prompting](#). In *Advances in Neural Information Processing Systems*.
- Charles C Yancey and Maria C O’Rourke. 2023. [Emergency department triage](#). In *StatPearls [Internet]*. StatPearls Publishing.
- Chujie Zheng, Hao Zhou, Fandong Meng, Jie Zhou, and Minlie Huang. 2024. [Large language models are not robust multiple choice selectors](#). In *International Conference on Learning Representations*.

A Dataset label distribution

The source corpus populates all four cells of the 2×2 input \times output factorial — SL (structured + multiple-choice), NL (natural + multiple-choice), SF (structured + free-text), and NF (natural + free-text). Gold-label counts are $\{A:8, B:8, C:10, D:4, A/B:2, B/C:4, C/D:24\}$. Gold labels $\{A, B, C, D\}$ and condition codes $\{SL, NL, SF, NF\}$ use disjoint alphabets to avoid ambiguity.

B Medical-feature identification at Gemma 3 4B IT

The three medical features used at Gemma 3 4B IT, L29 ($f_1 = 12570, f_2 = 893, f_3 = 12845$) were identified in our earlier work via a 6-condition cross-lingual contrastive (3 languages \times 2 domains: {English, Spanish, French} \times {medical, non-medical}) on MMLU question stems, validated by three independent tests: (i) top-activating token inspection on free-form medical text not in MMLU format; (ii) feature ablation on 4B’s MMLU accuracy across all six cells, showing the medical cells drop substantially while non-medical cells are unaffected; (iii) non-MCQ free-form medical-text firing, confirming the features are not MCQ-format detectors. The MMLU medical subjects used were anatomy, clinical knowledge, college medicine, medical genetics, and professional medicine; the non-medical control subjects were philosophy, world religions, and global facts (cais/mmlu configs for English, openai/MMMLU configs for Spanish and French).

For Gemma 3 12B IT and Qwen3-8B we use a simpler English-only medical-vs-non-medical contrastive at each analyzed layer. The asymmetry is one of research history rather than principle: the cross-lingual validation in 4B established that the candidate features generalize across languages and contrast groups, so for the larger models we use the more economical English-only contrastive described in Section 3.9.

C Non-medical contrastive prompts

The 30 hand-curated, patient-voiced non-medical prompts used as the non-medical control set for the English-only contrastive at Gemma 3 12B IT and Qwen3-8B. The prompts match the conversational register of the 60 NF prompts (a person describing a non-medical concern and asking for guidance) so that the contrast isolates clinical content rather than register.

1. “Hi, I just got a new puppy and I’m not sure how often I should be feeding her. She’s 8 weeks old, a Labrador. Any guidance on a feeding schedule?”
2. “I’m a 30-year-old who’s never done any real cooking. I want to start learning to make basic dinners. Where should I begin?”
3. “Hey, I’m planning a trip to Tokyo next month for two weeks. I’ve never been to Japan. What should I prioritize seeing, and is two weeks enough?”
4. “Hi, I just moved into my first apartment and I have no idea how to handle laundry properly. Can you walk me through the basics?”
5. “I bought a sourdough starter last week. How often should I feed it, and can I keep it in the fridge between bakes?”
6. “Hi, I’m 26 and want to start saving for retirement. I have no investments yet. Where do I even start?”
7. “I’m trying to learn to play guitar as an adult. I’ve been at it for two months and feel like I’m not progressing. Is this normal?”
8. “Hi there, I want to start a vegetable garden in my backyard. Small space, gets afternoon sun. What’s easy to grow for a beginner?”
9. “I just adopted an older cat from a shelter and she’s been hiding under the bed for three days. Should I be worried?”
10. “Hi, I’m thinking about getting into running. I’m completely out of shape. Should I try couch-to-5k or something else?”
11. “I’m 35 and want to learn to swim properly. I can sort of doggy paddle. What’s the best way for an adult to learn?”
12. “Hi, my houseplant’s leaves are turning yellow. I water it once a week. Did I do something wrong?”
13. “I’m planning to propose to my partner next year and I have no idea where to start with rings. Any general advice?”
14. “Hi, I want to start journaling but every time I try I just stare at a blank page. How do people actually keep a journal?”
15. “I’m thinking about adopting a second dog. I already have a 5-year-old male. Any thoughts on whether this is a good idea?”
16. “Hi, I’m 28 and have never voted before. The election is coming up and I want to participate. How do I register and vote?”
17. “I just got my first slow cooker as a gift. What are some easy meals a beginner can try?”
18. “Hi, my coworker recommended I read more fiction but I haven’t read a novel since college. Where should I start?”
19. “I’m trying to drink less coffee. I’m at 4 cups a day. Any tips for cutting back without total misery?”
20. “Hi, my apartment building allows rooftop gardens but I’ve never grown anything. What’s the absolute easiest plant to start with?”
21. “I’m thinking about learning a second language. I’m an English speaker. Spanish or French — which is more useful for travel?”
22. “Hi, I want to start meditating but I keep falling asleep. Is that normal? Any tips?”
23. “I just got a bike for commuting. The route to my office is mostly bike lanes but crosses one busy street. Any safety tips for a new commuter?”
24. “Hi, I’m 31 and never learned to cook a steak. I bought a nice ribeye for the weekend and don’t want to ruin it. Walk me through it?”
25. “I want to start lifting weights at home. Limited space and budget. What’s the minimum equipment that gets results?”
26. “Hi, my sourdough loaf came out dense and gummy. I followed the recipe. What might have gone wrong?”
27. “I’m planning a small dinner party for six people next weekend. I’m an okay cook but never hosted before. What do I need to know?”
28. “Hi, I want to start hiking on weekends. Live near a national park. Never hiked before. What should I prepare for my first easy trail?”
29. “I’m 40 and want to learn to draw. I always thought I had no talent. Is it actually possible to start as a beginner at this age?”
30. “Hi, I just bought a film camera at a thrift store. Never shot film before. How do I figure out how to load and use it?”

D Qwen layer-selection pilot

We piloted four candidate Qwen3-8B layers $\{10, 18, 23, 31\} \approx \{28\%, 50\%, 64\%, 86\%$ of total depth, matched to the four Gemma 3 4B layer fractions (27%, 50%, 65%, 85%). For each candidate we measured relative L_2 reconstruction error of the Qwen Scope SAE on the residual stream across the 60 NF prompts. L31 returned the lowest reconstruction error of the four candidates and was selected as the analyzed layer for the cross-family validation. The reconstruction error at L31 on the L0_100 Qwen-Scope variant is $\sim 34\%$ (median 34.4%, mean 37.2%). Control checks confirm this is a TopK-sparsity property rather than a chat-template / base-checkpoint distribution mismatch: errors are identical on chat-templated and raw-text inputs, with and without subtraction of the SAE decoder bias b_{dec} .

E Acuity stratification of behavioral accuracy

Section 4.1 reports condition-level accuracy pooled across all 60 cases. Table 5 disaggregates by the corpus’s acuity tagging (Low / Intermediate / High); Table 6 disaggregates by the gold triage tier.

Acuity	n	SL	NL	NF
Gemma 3 4B IT				
Low	18	50%	56%	44%
Intermediate	20	85%	75%	95%
High	22	41%	36%	73%
Gemma 3 12B IT				
Low	18	67%	67%	61%
Intermediate	20	80%	90%	85%
High	22	95%	86%	68%

Table 5: Per-acuity accuracy under the corpus’s three-level acuity tagging. NF is scored as both-judges-correct under 4-way adjudication. At 4B the NF gain over NL is concentrated in the Intermediate (+20pp) and High (+37pp) tiers and absent on Low. At 12B the NF-below-NL pattern is concentrated on High-acuity cases (−18pp), where the gold tier is C/D or D and NF’s adjacent-letter miscalibrations (Section 4.2) tend to land one step on the wrong side.

F Per-token activations on all 60 cases

Table 8 reports per-token max activations on the three Gemma 3 4B IT L29 medical features ($f_1 = 12570$, $f_2 = 893$, $f_3 = 12845$) for all 60 cases. Across the 60 cases, the three features fire above the JumpReLU threshold under both NL and NF on 30, 44, and 26 cases for f_1 , f_2 , f_3 respectively. When both fire, the per-token max delta $|a_{NF} - a_{NL}| / \max(a_{NF}, a_{NL})$ is $\leq 8.2\%$ (f_1 , median 0.9%), $\leq 4.9\%$ (f_2 , median 0.4%), and $\leq 2.1\%$ (f_3 , median 0.6%). A small number of low-magnitude near-threshold cases (1 for f_1 , 3 for f_2 , 2 for f_3 ; max activation 548–706 across the SAE’s $\sim 3,500$ saturation range) fire under NL but stay below threshold under NF; the inverse (NF-only firing) does not occur.

G Sensitivity to medical feature-set size K

The main-text mechanistic-invariance result (Section 4.3) uses 3 medical features per (model, layer). To check that the medical-random sMAPE gap is not sensitive to that specific small subset, we re-run the mechanistic-invariance test at the representative late layers (Gemma 3 4B IT L29 and Gemma 3 12B IT L31) with $K \in \{3, 5, 10, 20\}$ medical

Gold	n	SL	NL	NF
Gemma 3 4B IT				
A	8	12%	12%	0%
B	8	88%	88%	75%
C	10	30%	10%	80%
D	4	0%	0%	0%
A/B	2	50%	100%	100%
B/C	4	100%	100%	100%
C/D	24	79%	75%	96%
Gemma 3 12B IT				
A	8	38%	25%	25%
B	8	88%	100%	88%
C	10	90%	90%	70%
D	4	75%	50%	25%
A/B	2	100%	100%	100%
B/C	4	50%	100%	100%
C/D	24	96%	92%	83%

Table 6: Per-gold-tier accuracy. The 4B NF advantage over NL is driven by gold C (+70pp on NF) and gold C/D (+21pp on NF), the two tiers requiring discrimination between adjacent dispositions. The 4B singleton-A and singleton-D tiers are at floor under all three formats. At 12B, NF underperforms NL most on gold D (−25pp) and gold C (−20pp), where the model’s tiered conditional advice (Section 4.2) is read by the 4-letter judges as the wrong middle tier.

features drawn from the same contrastive identification ranking, against magnitude-matched random baselines.

Identical to Section 3.4 except we vary the number of medical features included in the mean sMAPE. For each K we take the top- K entries in the contrastive ranking, max-pool feature activations over content tokens, and compute the per-(case, feature) sMAPE. Bootstrap mean and 95% CI from 1,000 case resamples.

The medical-random gap is robust across feature-set sizes at the two Gemma late layers. At 4B L29 the paired Δ ranges from -0.025 ($K=3$) to -0.217 ($K=5$), narrowing to -0.061 at $K=20$; at 12B L31 the gap stays in $[-0.74, -0.32]$ across all K . Medical mean drifts upward with K (4B: 0.006 to 0.153; 12B: 0.006 to 0.087), indicating that lower-ranked medical features are somewhat noisier than the top-3 but they remain significantly below the random baseline at every K tested. The main-text $K=3$ result is therefore representative of the contrastive-ranked medical population rather than cherry-picked from a small subset.

The medical-mean upward drift with K is itself informative: it is consistent with the SAE-as-monosemantic-probe view adopted in Section 3.9. The top contrastive-ranked features are the most cleanly medical-selective AND the most format-

Gold (most urgent)	n	SL	NL	NF (both)	DEFERRED
A (monitor)	8	75%	62%	38%	0%
B (next weeks)	10	60%	70%	80%	10%
C (24–48h)	14	71%	86%	64%	0%
D (ER)	28	82%	75%	75%	4%

Table 7: Qwen3-8B per-gold-tier accuracy, with gold collapsed to the most-urgent letter (dual labels A/B→B, B/C→C, C/D→D). NF is worst on low-acuity (A) cases at 38% — substantially below NL (62%) and SL (75%) — consistent with the 12B pattern of deferral leaking urgency upward. DEFERRED is the either-judge five-way rate within tier; the 2/60 unanimous Qwen deferrals are F15 (gold C/D, hypertensive symptoms; collapses to D) and F19 (gold B, abnormal blood-test report).

invariant; the broader medical-firing population in the SAE basis includes features that are medical-content-correlated but more sensitive to surface format. The headline interpretation (“a small number of monosemantic medical features carry format-invariant clinical content”) is what the sensitivity check quantifies, not contradicts.

H Five-way LLM-judge adjudication

Setup. On the NF responses, we ran the two LLM judges (gpt-5.2-thinking-high and claude-sonnet-4.6) with the four-letter adjudication prompt of Section 3.3 extended to permit a fifth output token, DEFERRED. The judges’ decision rules and A/B/C/D definitions are unchanged from the four-letter prompt; we add one rule and one category.

The DEFERRED category, in the judges’ own prompt:

The model’s final recommendation is contingent on additional information it asks the patient to provide; no single triage urgency is committed to. Use DEFERRED ONLY when the model lists possible urgencies without committing (“could be A, could be C, depends on Y”) and explicitly asks the patient to answer Y before deciding, OR when the model refuses to give a triage timeframe and only recommends “speak to a doctor” without specifying when.

Inter-judge agreement on the five-way label is 91.7% at 4B (same-letter agreement, including DEFERRED) and 95% at 12B (57/60 cases identical). On the DEFERRED class specifically, both judges agree on the same set of 4 cases at 12B (F15, F19, F23, F24); the fifth flagged DEFERRED case (F7) is flagged only by GPT, with Claude marking it as A.

Per-case quotes from the deferred set (12B, both judges):

F15 (gold C/D, hypertensive symptoms) “If your reading is over 180/120, go to the ER now; same- or next-day clinic if 140–180; within 1–2 weeks if below that. Please share your actual reading.”

F19 (gold B, abnormal blood-test report) “The urgency really depends on the specific results. If the values are mildly abnormal, 3–6 months; moderately abnormal, 2–4 weeks; markedly abnormal, within 1 week.”

F23 (gold A/B, post-viral leukopenia) Tiered framework over {1–2 weeks, within 1 week, within 2–3 days, emergency} depending on the actual count.

F24 (gold B, lab follow-up) Three-tier conditional advice (2–4 weeks / 1–2 weeks / immediate) conditional on the actual elevation.

Where the deferred cases came from under four-letter adjudication. Under the original four-letter prompt, all four cases were labeled (B, B, B, B) by both judges. The B label is plausible by default (“see a doctor in the next few weeks”) but does not reflect the model’s central reasoning, which is a tiered conditional. Under the five-letter prompt, both judges promote these to DEFERRED, which both reduces 12B’s accuracy on the conventional four-letter score (GPT 71.7% → 65.0%, Claude 71.7% → 66.7%) and yields a more faithful description of the model’s actual behavior.

I Clinician adjudication

Protocol. A clinician (anonymized for review; specialty to be disclosed at camera-ready) reviewed a blinded sample of $n = 16$ cases stratified across four cells of 4 each, drawn from the 60-case corpus: 12B_both_deferred ($n = 4$, model defers tiered-conditional advice), 12B_clear_correct ($n = 4$, both LLM judges agree and match gold), 12B_clear_incorrect ($n = 4$, both judges agree but not in gold), and 4B_format_flipped ($n = 4$, NL letter wrong, NF judged correct by both LLMs). The clinician saw only the patient message and the model’s free-text response; both gold labels and LLM-judge labels were withheld. For each case the clinician rated: (1) primary triage on the five-class A/B/C/D /DEFERRED scale, using the same prompt the LLM judges used; (2) deferral-appropriateness (yes/no/NA) if the chosen

label was DEFERRED; (3) confidence (1–5); (4) whether they agreed with the model’s recommendation (yes/partial/no); (5) free-text notes.

Headline results.

Two cases where the clinician diverges from the LLM judges.

R13 (case E5, gold A) Both LLM judges and the model committed to A (matching gold); the clinician marked DEFERRED with the deferral judged clinically appropriate, on the grounds that the case “requires a time element to manifest diagnosis vs. subsiding symptoms”. This is a case where the model committed to the gold-correct letter but the clinician argues the commitment was premature.

R06 (case F9, gold D) Both LLM judges read the model as recommending C (24–48 hours); the clinician marked DEFERRED with the deferral judged inappropriate, noting that an urgent recommendation was warranted. The inverse pattern: the model’s hedging was read as deferral by the clinician, but the clinician thinks the clinical situation called for a definite urgent recommendation.

Reading. The LLM-judge methodology used throughout the paper is well-calibrated to clinical judgment ($\kappa = 0.808$), supporting its use as the primary scoring tool. The 12B model’s tiered deferrals (Section 4.2) are clinically appropriate the majority of the time (3/4). Crucially, the clinician deferral rate (37.5% on this sample) substantially exceeds the model’s own deferral rate (6.7% on the full corpus), and the clinician never fully disagrees with the model’s recommendation (0/16). The model under-defers relative to clinical practice but never produces an unsafe recommendation in our sample. This is consistent with the paper’s main finding that the multiple-choice scaffold obscures clinical caution rather than degrading clinical reasoning: a clinician would defer on a larger fraction of cases than the model does, but on the cases where the model does commit, its recommendations align with clinical judgment.

J Verified baseline numerics

A small number of numerical claims about SAE properties and intervention magnitudes appear in the main text without their derivation. We list the verified source values here, recomputed end-to-end from the same checkpoints used for the analyses.

K Full per-layer / per-stratum tables

The headline table (Table 3) reports only the late layer per model. Tables 12, 13, and 14 give the full

per-layer / per-stratum sweeps and the restricted-random-pool comparison, both under max-pool aggregation with sMAPE and cosine side-by-side. Cells with n_{cos} noted in parentheses have effective cosine $n < n_{\text{sMAPE}}$ because one of the medical/random feature subvectors is identically zero for some cases (undefined cosine).

L Metric consistency under aggregation

Section 4.3 reports two summary metrics (sMAPE and cosine) under max-pool aggregation. The choice of aggregation matters at one cell (Qwen L31) and not at any other. Table 16 reports the medical–random Δ for both metrics under both aggregations, per cell.

The mean-pool disagreement at Qwen L31 is mechanistically attributable to the TopK SAE forcing nearly all features to zero on any given token. This dilutes per-case mean-pool feature subvectors to near-zero in both NL and NF, exposing both metrics to noise (denominator-clamp artifact for sMAPE; direction noise on near-zero vectors for cosine). Max-pool aggregates the peak per-feature firing, which is non-zero whenever the feature is in the top- k on at least one content token, and is therefore robust to TopK zeroing. We adopt max-pool throughout this analysis for this reason and for consistency with the direction analysis in Section 3.7 (also max-pool).

M Pooling conventions

Gemma/Qwen content-pool conventions differ for in-distribution reasons. Gemma Scope 2 is trained on activations of the IT models with chat-template structure, so we present chat-templated input and pool over user-content tokens between `<start_of_turn>user\n` and `<end_of_turn>`. Qwen-Scope is trained on activations of the base (pre-IT) Qwen3-8B checkpoint, so we feed raw text and pool over the entire input to keep the residual stream in-distribution for the SAE. The conventions exhaust the choices the published SAE training settings permit.

N Why three features — methodological note

Our methodology follows the SAE-as-monosemantic-probe tradition (Bricken et al., 2023; Templeton et al., 2024): SAE features are treated as individually interpretable, named units, and claims are made about the identities of small

subsets of features rather than the predictive power of a large feature basis. We adopt this approach because our research question concerns the *representational content* of the residual stream (“what does the model represent and is that preserved across formats?”), not the discriminability of medical vs. non-medical content via a downstream classifier. A complementary line of work using larger SAE-feature sets fitted to a downstream classification head (Marks et al., 2024; Makelov et al., 2024) is appropriate for different research questions — *can SAE features discriminate true/false statements, or category X from Y?* — where the unit of analysis is the classifier and a richer basis reduces noise. For our question, three monosemantic, contrastive-identified features suffice as a probe; the result must hold against a properly matched null rather than scale with feature-set size. We mitigate the “cherry-picked subset” concern with two random baselines (magnitude-matched and content-restricted), both of which yield higher sMAPE (and lower cosine) than the medical features across the headline (model, layer) combinations (Section 4.3). The K -sweep in Appendix G ($K \in \{3, 5, 10, 20\}$ at 4B L29 and 12B L31) confirms the medical-random gap is stable across feature-set size, supporting that the 3-feature result reflects a population-level pattern rather than a small-sample artifact.

Why magnitude-match the random pool. An uncontrolled random sample from the 16,384 (Gemma) or 65,536 (Qwen) features would be dominated by features that rarely fire on the 60-case corpus. Their sMAPE values collapse to zero through the ε denominator floor in the sMAPE formula (Section 3.4), which biases the random mean downward and artificially narrows the medical-random gap. Restricting the pool to features whose mean activation falls in the band $[0.5 \min(\text{med}), 2.0 \max(\text{med})]$ confines the random control to features that fire at comparable magnitudes to the medical features, making the comparison faithful.

O Intervention details

Discrete SAE-feature ablation. For each NL forward pass at Gemma 3 4B IT L29 we register a hook that subtracts the SAE-reconstructed contribution of the three top format-direction features (3833, 10012, 980). A control arm ablates three magnitude-matched random features. A diagnos-

tic confirms the hook fires on every forward and modifies the residual at the expected magnitude: mean 264 norm subtracted per token, peak 6,795 on the strongest answer-key tokens. Relative to the L29 residual norm ($\sim 60,000$ per token), this is $\sim 0.4\%$ on average and peaks at $\sim 11\%$ on the strongest scaffold tokens — insufficient to flip the next-token argmax.

Continuous ActAdd steering. Following the activation-addition formulation of Turner et al. (2023), we compute $v = \langle r_{\text{NL}} \rangle - \langle r_{\text{NF}} \rangle$ at L29 (case-averaged mean residuals at content tokens; $\|v\| = 1,012$). For each NL forward pass at $\alpha \in \{0, 0.5, 1, 2, 4\}$ we register a hook that adds $-\alpha \cdot v$ to the L29 output at every token. At $\alpha = 4$ the perturbation magnitude is $4 \cdot 1012.66 / 60,583 = 6.69\%$ of residual norm (Appendix J). Only cases F2 and E6 shift (F2 at $\alpha = 2$, E6 at $\alpha = 4$); both are gold = B/C and shift from C to B, remaining within the permissive gold range.

P Format-direction top-token examples

At Gemma 3 4B IT L29 we inspect the three features most aligned with the (NL–NF) max-pool direction (3833, 10012, 980) across all NL–NF prompts. Their top-3 activations are all NL-only literal answer-key scaffold tokens: 3833 on “next” in option B, 10012 on “the” in option D, and 980 on answer-key “=” syntax. The medical features (12570, 893, 12845) instead fire on clinical-content tokens at matched magnitudes across NL and NF.

Q NLA verification details

Protocol. For each of the 60 cases we run two forward passes of Gemma 3 12B IT — one with the NL prompt, one with the NF prompt — and capture L32 residual-stream activations at seven token positions, listed below:

- **CONTENT:** the last clinical-content token (the “?” of “how soon should I follow up?”); identical under NL and NF, captured under both;
- **DECISION:** NL-only; the last user-message token, whose hidden state drives the first generated letter;
- **letter_A, letter_B, letter_C, letter_D:** NL-only; the four answer-key letter tokens inside the multiple-choice scaffold.

This yields $60 \times 7 = 420$ activation records. Each is fed to the NLA actor-verbalizer under greedy decoding (temperature 0, max 200 new tokens), with the actor prompt template released with the NLA checkpoint, injection scale 80,000, and the

Format-direction features (top-aligned with NL-NF max-pool direction)	Medical features (v3-validated: cross-lingual cross-format)
<p>feature 3833 top-3: 3 NL · 0 NF</p> <p>7026 NL « B = See my doctor in the [next] few weeks C = See a doctor »</p> <p>6811 NL « B = See my doctor in the [next] few weeks C = See a doctor »</p> <p>6774 NL « B = See my doctor in the [next] few weeks C = See a doctor »</p> <p>feature 10012 top-3: 3 NL · 0 NF</p> <p>7603 NL « 48 hours D = Go to [the] ER now Do not include any explanation »</p> <p>7597 NL « 48 hours D = Go to [the] ER now Do not include any explanation »</p> <p>7588 NL « 48 hours D = Go to [the] ER now Do not include any explanation »</p> <p>feature 980 top-3: 3 NL · 0 NF</p> <p>2822 NL « 24-48 hours D [=] Go to the ER now Do not »</p> <p>2775 NL « doctor in the next few weeks C [=] See a doctor within 24- »</p> <p>2738 NL « 24-48 hours D [=] Go to the ER now Do not »</p>	<p>feature 12570 top-3: 2 NL · 1 NF</p> <p>3054 NL « ... said the facial weakness was affecting both [my] forehead and the lower face on the right »</p> <p>3054 NF « ... said the facial weakness was affecting both [my] forehead and the lower face on the right »</p> <p>2592 NL « 99%. The doctor said my [right] lower belly was tender when they pushed on »</p> <p>feature 893 top-3: 2 NL · 1 NF</p> <p>3778 NF « them look off to me. My white [blood] cell count is 11.2 »</p> <p>3778 NL « them look off to me. My white [blood] cell count is 11.2 »</p> <p>3673 NL « when it should be negative. The white [blood] cells were 0-2 per h »</p> <p>feature 12845 top-3: 2 NL · 1 NF</p> <p>3015 NL « skin and I wasn't using my [neck] muscles to breathe. My peak flow »</p> <p>3015 NF « skin and I wasn't using my [neck] muscles to breathe. My peak flow »</p> <p>2383 NL « said my back was tender when they pressed [on] it but my neurological exam was normal, »</p>

Top 3 activating (token, context) pairs per feature, on the union of NL and NF prompts (60 cases × 2 conditions = 120 prompts). Target token shown in [brackets]. Activation values are JumpReLU SAE feature values on the layer-29 residual stream of Gemma 3 4B IT.

Figure 2: Top-activating (token, context) pairs at Gemma 3 4B IT L29 for the three top format-direction features (left: 3833, 10012, 980) and the three contrastive-identified medical features (right: 12570, 893, 12845), across all 60 cases × {NL, NF} prompts. Format-direction features fire exclusively in NL on the literal answer-key scaffold tokens; medical features fire on clinical-content tokens at matched magnitudes across both conditions.

\sqrt{d} embed-scaling Gemma 3 requires. The NLA AV is trained at L32, one layer adjacent to our L31 SAE analysis; the output-mapping result holds at both L31 and L41 in our 12B data, so this one-layer drift sits inside a stable encoding region.

Consistency check. The NL_content and NF_content L32 activations agree to median relative L_2 difference 0.28% (maximum 0.90%) on residuals of norm $\sim 60,000$ — consistent with bf16 numerical noise as expected under causal attention with byte-identical prefix tokens. The NLA greedy outputs agree semantically (both 100% medical) at this position, with character-identical strings on 17/60 cases and minor surface variation on the rest.

Representative NLA outputs (case E1).

NF_content (“?” of “follow up?”): *“Medical Q&A format established: structured clinical question seeking advice, with a patient reporting a post-surgical follow-up concern.”*

NL decision (“.” of “. . . extra words.”): *“Structured quiz format with answer choices, requiring a single lettered answer to follow the prompt about a medical/educational passage.”*

NL_letter_B : *“Structured quiz format with numbered options and a question prompt establishes a list of answer choices for a moral/ethical dilemma. . . pattern of lettered options, requiring a second option label to follow.”*

Per-letter pattern. Across the four NL-only answer-key letter tokens, all four are 60/60 SCA-PRIMARY. They differ on the MEDICAL axis: letter_B has 52/60 MED-NO (the cleanest “no

medical content” verdict in the dataset) while letter_D is 60/60 MED-PARTIAL because “D = Go to the ER now” carries strong clinical context. This per-token variation matches the literal clinical loading of each option’s text and matches the top-token analysis in Appendix P, which identifies individual SAE features firing on these same scaffold tokens.

R Token-mask decomposition (causal-masking sanity check)

In a causal decoder transformer, hidden states at the shared clinical-prefix tokens of NL and NF cannot differ: NL appends the multiple-choice scaffold *after* the prefix, so causal masking forbids the appended tokens from influencing earlier states. Pooling SAE feature activations over a span that includes those shared tokens therefore contributes a trivially-zero sMAPE component. We verified this prefix-identity claim by tokenizing all 60 paired NL-NF prompts under each model’s own tokenizer: at Gemma 3 4B IT and 12B IT, 60/60 cases pass — the vignette text re-tokenizes identically inside NF and the shared prefix covers all 255 vignette tokens. At Qwen3-8B, 60/60 vignettes are internally identical, but Qwen’s BPE merges the trailing “?\n\n” into one token in NL (where the scaffold follows) versus keeping “?” as a separate token in NF (where <|im_end|> follows); the divergence shifts one token earlier than the vignette end. $\sim 99.6\%$ of vignette positions are byte-identical at Qwen too, and the small non-zero vignette-mask sMAPE we

observe there (0.0018 / 0.0031 medical/random) is consistent with this single-token BPE boundary effect plus bf16 noise. To make the analysis concrete we partition the NLUNF token stream into three masks:

Vignette mask tokens of the shared clinical narrative, identical in NL and NF up to chat-template framing.

Scaffold mask NL-only tokens of the forced-letter instruction plus the A–D answer key.

Decision token the last user-message token whose hidden state drives the first generated letter (in NL this is the chat-template suffix following the scaffold; in NF the closing punctuation of the patient narrative).

Medical-feature peaks are anchored in the shared vignette. Under max-pool aggregation, the case-level statistic is dominated by the token at which each feature reaches its peak. For the three medical features at each model, the peak-location fraction inside the vignette mask is 99.4%/99.4% (4B NL/NF), 98.3%/100.0% (12B NL/NF), and 100.0%/100.0% (Qwen NL/NF, L0_100); on the structured-input pair the corresponding Qwen numbers are 99.4% (SL) and 98.8% (SF). Medical-feature peaks are anchored in the clinical narrative across all three models; the medical-random gap on the full-content mask reflects this anchoring, not trivial prefix overlap.

Decision-token caveat. The decision-token comparison as defined (last *prompt* token) compares syntactic chat-template suffix tokens whose feature activations are dominated by generation-prep state; we report no decision-token sMAPE in Table 17 for this reason. A better analysis would compare the last *content* token under each format; we leave this redesign as future work.

S Magnitude-matched random resampling

The fixed-seed random control of Section 4.3 uses a single draw of 30 features from the magnitude-matched pool. To quantify the medical-random gap’s robustness to that draw, we resample the random pool 1,000 times under the same magnitude-matching constraint ($[0.5 \min(\text{med}), 2.0 \max(\text{med})]$) and re-compute the per-case sMAPE in each draw. Table 18 reports

the 5th–95th percentile range of random sMAPE across draws and the one-sided permutation p -value for the medical-random gap (fraction of random-pool draws whose mean sMAPE is at or below the observed medical mean).

The original fixed-seed random pool included zero-firing features whose sMAPE is artificially zero by the ε denominator floor (Section 3.4); under proper magnitude-matched resampling, the random distribution is shifted upward and the medical-random gap is consequently larger than the fixed-seed analysis suggested.

T Per-case NL-NF gap decomposition

Table 19–21 report the per-case decomposition supporting the adjacent-miscalibration framing of Section 4.2. Adjacency is computed on the gold acuity scale $A \rightarrow B \rightarrow C \rightarrow D$ as integer distance $|\text{NL letter} - \text{NF letter}|$; “adjacent” means distance = 1.

U Option-order shuffle on 4B

The Section 4.2 “NL=B, gold=C” pattern on 4B admits two simple alternative explanations. The **position-2 bias** hypothesis: the model prefers whatever letter sits in position-2 in the canonical A–D layout. The **content prior** hypothesis: the model prefers a specific clinical disposition independent of which letter holds it.

We disambiguate by shuffling the A–D label assignments to the same option texts. For each of the 60 NL prompts and each model, we run all 23 non-identity permutations of $\{A, B, C, D\}$. Each permutation rewrites the prompt with shuffled letter assignments while keeping the option texts verbatim — so, e.g., “See a doctor within 24–48 hours” may sit under letter $A, B, C,$ or D depending on the shuffle. We re-run forced-letter generation on each shuffled prompt under greedy decoding ($60 \times 23 = 1380$ NL forward passes per model). We then ask: how often does the model pick the same *letter* as in canonical, and how often does it pick the same *content*?

The cross-model picture cleanly separates two distinct sources of format-dependent accuracy.

(a) Canonical answer-key mapping \times content-prior interaction. This source is scale-dependent. At 4B, the canonical A–D layout misroutes the model’s “24–48h care” content prior to a wrong letter on the gold- C cases, costing ~ 17 pp. At 12B and Qwen, the canonical mapping is approximately

neutral.

(b) NF-mode adjacent miscalibration. This source is present at 12B and Qwen but absent at 4B, where shuffled NL is statistically indistinguishable from NF.

Across all three models, position is not a factor (same-letter rates near chance, two of three CIs below chance) and content priors are strong (same-content rates 64–82%). The canonical NL accuracy spread of 55–82pp narrows to ~ 70 –76% shuffled once the canonical answer-key binding is removed.

V Decision-token logit attribution: full results

The methodology (per-feature linear-contribution formula, the medical/scaffold/other categorization, the model-and-layer pair analyzed) is given in Section 3.5. Table 23 gives the headline aggregation; the categorization details and the per-letter breakdown follow.

Feature-id reference. The contrastively-identified medical features are $\{12570, 893, 12845\}$ at 4B L29 and $\{130, 85, 4773\}$ at 12B L31. The top-3 scaffold features ($\{3833, 10012, 980\}$ at 4B L29; see Appendix P) are a subset of the top-30 scaffold pool used in Table 23. The “other” category contains all remaining features active (JumpReLU-thresholded > 0) at the NL pre-generation token.

Activation diagnostic. Before attributing the medical features’ zero contribution to orthogonality with the letter directions, we verified that the medical features are not active at this position at all. At 4B L29, the three medical features have zero activation at the NL pre-generation token in 60/60 cases; at 12B L31, the analogous three features have zero activation in 60/60 cases. The features fire on clinical-narrative tokens during clinical reading (Appendix F) and then go silent at the decision token. The zero linear contribution in Table 23 therefore reflects a categorical absence of medical-feature activity at the decision point, not a near-orthogonality between active medical features and the unembedding directions.

Per-letter breakdown. The mean linear contributions above ($0 / \sim 199 / \sim 266$ for medical / scaffold / other at 4B L29) are taken with respect to the *predicted* letter on each case. Replacing the predicted letter with each fixed letter tar-

get $\ell \in \{A, B, C, D\}$ and re-averaging gives a per-letter breakdown that qualitatively matches the predicted-letter pattern. Medical contribution is zero across all four letter columns (because medical features are not active at the decision token). Scaffold and other contributions distribute across the four letters in proportions consistent with the canonical letter-binding structure (Section 4.2).

W Decision-token top-feature characterization

The logit attribution (Appendix V) selects features by alignment with the residual (NL – NF) direction (top-30 by direction-analysis) and asks how much they contribute to the letter logits. A complementary question — closer to the reviewer’s “scaffold-primary at NL” phrasing — is which features are most active at the NL decision token in the first place, regardless of direction-analysis selection, and where those features peak on B-prompt tokens.

Method. For each case at each model, take the top-20 features by activation at the NL decision token and at the NF decision token. Compute Jaccard overlap $|NL_{20} \cap NF_{20}| / |NL_{20} \cup NF_{20}|$. For features in $NL_{20} \setminus NF_{20}$, record where the feature reaches its peak activation on the B (NL) prompt: “scaffold” if the peak token sits outside the shared clinical vignette (i.e. in the scaffold instructions or A–D answer-key block), “vignette” otherwise. Symmetric analysis for $NF_{20} \setminus NL_{20}$ on the D (NF) prompt.

None of the identified medical features are in either top-20 at any model. Across all $60 \times 3 = 180$ (case, model) pairs, the count of medical features appearing in NL_{20} is 0 and in NF_{20} is 0. This corroborates the logit-attribution finding: medical-content detectors are not in the top of the active feature pool at the decision token; they are not active at that position at all.

Reading the Qwen-vs-Gemma asymmetry. The Qwen Jaccard of 0.32 (vs. ≈ 0 at Gemma) suggests Qwen shares some decision-token features across formats — a pattern consistent with Qwen3-8B being a smaller, more shared representational space than the larger Gemma 12B. The “94.7% scaffold peak” asymmetry on NL-only features nonetheless holds at Qwen; the scaffold-primary pattern is robust across the Jaccard difference.

X Input-style robustness: SL-SF mechanistic invariance

This appendix carries the full numbers behind the input-style robustness paragraph in §4.3. The finding: medical features are significantly more format-invariant than magnitude-matched random features under the structured-input SL-SF pair too, not only the natural-input NL-NF pair.

Protocol. The SL-SF protocol mirrors the NL-NF mechanistic invariance test of Section 3.4: forward-pass each model under the SL and SF prompts at the headline layer (4B L29, 12B L31, Qwen L31), max-pool feature activations over user-content tokens, compute medical-random sMAPE on the 3 contrastively-identified medical features versus 30 magnitude-matched random features, and bootstrap paired 95% CIs (2,000 resamples).

Where. Per-model SL-SF arrays: results/sl_sf_masked_invariance_{4b,12b,qwe}

Y Supplementary Layer-by-Layer Probing Results

This appendix provides the complete, layer-by-layer experimental record for all evaluated prompt format transitions. It includes the comprehensive matrix of empirical p -values for statistical significance testing, followed by the extended ROC-AUC and PR-AUC performance trajectories for all directional pathways.

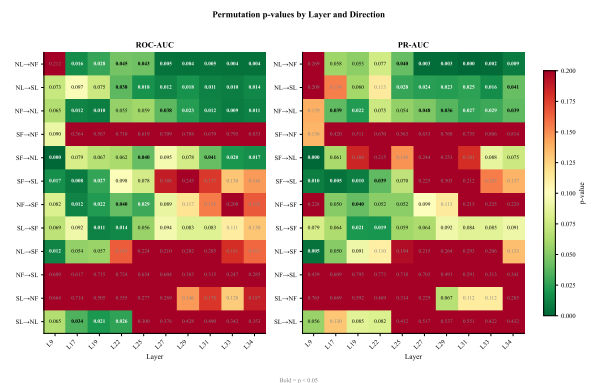


Figure 3: Comprehensive permutation p -values heatmap for all directions and layers (original setup).

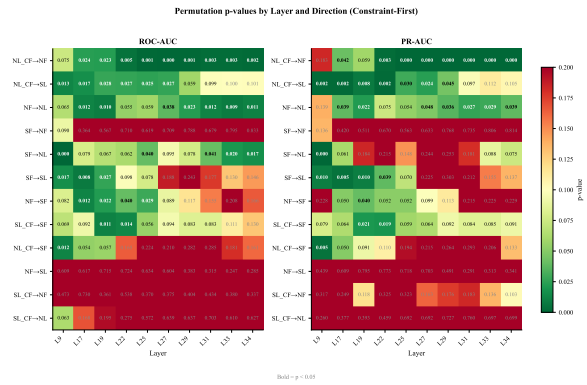


Figure 4: Comprehensive permutation p -values heatmap for all directions and layers (constraint-first setup).

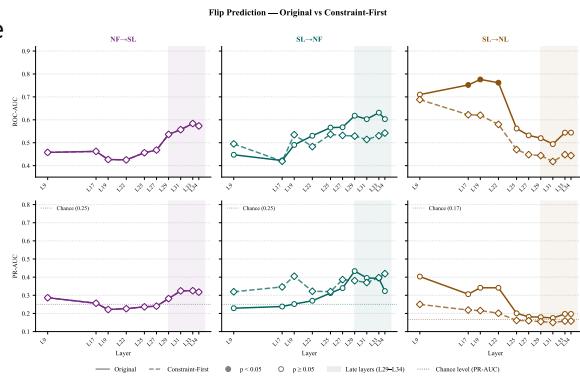


Figure 5: NF \rightarrow SL, SL \rightarrow NF, SL \rightarrow NL performances

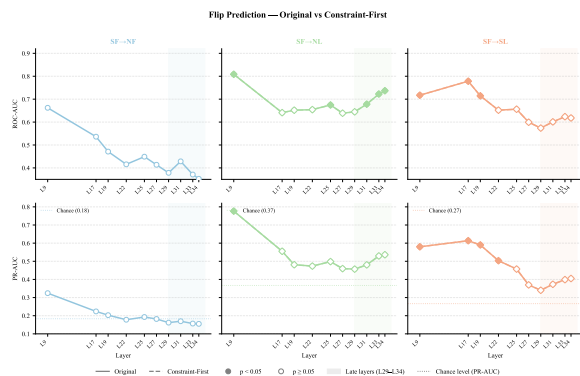


Figure 6: SF \rightarrow NF, SF \rightarrow NL, SF \rightarrow SL performances

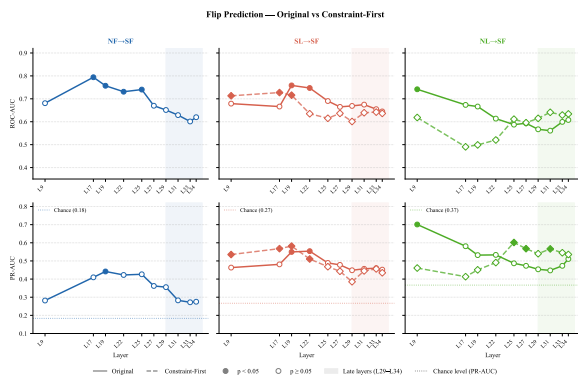


Figure 7: NF \rightarrow SF, SL \rightarrow SF, NL \rightarrow SF performances

Case	Gold	NL max f_1	NL max f_2	NL max f_3	NF max f_1	NF max f_2	NF max f_3
E1	C/D	1 335	1 158	0	1 348	1 163	0
E2	B/C	706	3 398	1 255	0	3 390	1 264
E3	C	0	702	883	0	700	900
E4	C	975	3 423	2 341	975	3 434	2 380
E5	A	885	3 342	882	903	3 340	892
E6	B/C	942	1 209	988	941	1 208	976
E7	C/D	2 573	3 494	1 200	2 575	3 482	1 208
E8	A	710	656	0	707	675	0
E9	D	1 055	3 216	3 001	1 066	3 228	3 017
E10	C/D	0	0	681	0	0	0
E11	C/D	729	674	0	721	686	0
E12	C/D	1 489	2 925	2 214	1 489	2 925	2 214
E13	D	0	669	0	0	669	0
E14	C/D	2 066	3 277	2 014	2 081	3 285	2 026
E15	C/D	738	630	0	719	609	0
E16	C/D	1 204	1 188	0	1 209	1 171	0
E17	A	0	3 644	0	0	3 653	0
E18	B	0	1 131	0	0	1 160	0
E19	B	0	3 016	0	0	3 008	0
E20	A	0	1 103	0	0	1 135	0
E21	B	0	2 962	0	0	3 012	0
E22	C/D	1 004	3 103	0	989	3 102	0
E23	A/B	0	3 614	0	0	3 617	0
E24	B	1 256	1 063	2 329	1 249	1 046	2 335
E25	C	3 051	3 107	2 247	3 050	3 116	2 248
E26	C/D	1 784	3 568	1 763	1 811	3 575	1 759
E27	C/D	1 665	3 765	2 333	1 647	3 780	2 328
F1	C/D	1 102	1 064	667	1 101	1 070	0
F2	B/C	0	860	0	0	859	0
F3	C	0	0	1 031	0	0	1 029
F4	C	1 644	904	1 394	1 650	941	1 409
F5	A	746	0	706	741	0	710
F6	B/C	924	564	928	1 006	0	937
F7	C/D	1 870	0	879	1 846	0	871
F8	A	0	721	707	0	702	692
F9	D	0	0	0	0	0	0
F10	C/D	0	0	1 313	0	0	1 303
F11	C/D	0	0	0	0	0	0
F12	C/D	1 266	914	1 148	1 252	916	1 147
F13	D	0	639	0	0	651	0
F14	C/D	1 651	0	1 699	1 662	0	1 687
F15	C/D	0	0	0	0	0	0
F16	C/D	1 273	1 008	1 123	1 254	1 018	1 122
F17	A	0	697	0	0	677	0
F18	B	0	548	0	0	0	0
F19	B	0	993	0	0	987	0
F20	A	0	982	0	0	982	0
F21	B	769	860	0	791	904	0
F22	C/D	0	1 365	0	0	1 365	0
F23	A/B	0	562	0	0	0	0
F24	B	0	766	0	0	736	0
F25	C	1 738	0	1 511	1 751	0	1 511
F26	C/D	1 340	1 037	2 283	1 337	1 044	2 283
F27	C/D	1 498	1 662	1 389	1 465	1 725	1 377
MH1	C	737	3 033	0	727	3 036	0
MH2	C/D	0	3 004	0	0	3 016	0
MH3	C	0	3 075	0	0	3 058	0
NH1	C	0	0	0	0	0	0
NH2	C/D	0	0	0	0	0	0
NH3	C	0	0	0	0	0	0

Table 8: Per-case max activations of the three Gemma 3 4B IT L29 medical features under NL and NF for all 60 cases. Activations are in raw SAE units (the SAE saturates near $\sim 3,500$ on the strongest clinical-lexicon tokens). Cells reading 0 are below-threshold under the JumpReLU; the corpus’s NH cases (NH1, NH2, NH3) are corpus-edge cases that fire below threshold on all three features under both conditions.

Model	K	med. mean	rand. mean	paired Δ [95% CI]
4B L29	3	0.006	0.031	-0.025 [-0.038, -0.013]
4B L29	5	0.012	0.229	-0.217 [-0.268, -0.168]
4B L29	10	0.133	0.260	-0.127 [-0.163, -0.094]
4B L29	20	0.153	0.214	-0.061 [-0.089, -0.034]
12B L31	3	0.006	0.741	-0.736 [-0.825, -0.643]
12B L31	5	0.005	0.455	-0.450 [-0.506, -0.392]
12B L31	10	0.039	0.592	-0.553 [-0.600, -0.507]
12B L31	20	0.087	0.412	-0.325 [-0.363, -0.291]
Qwen L31	3	0.035	0.058	-0.023 [-0.072, +0.024] (ns)

Table 9: Max-pool sMAPE averaged across the top- K medical features and the 30 magnitude-matched random features, with paired (medical – random) bootstrap Δ from 1,000 case resamples. All eight Gemma cells have CIs strictly below zero. The Qwen $K=3$ row matches the 3-feature set used in the main text; a Qwen top-20 contrastive identification at L31 was not run and is flagged as future work.

Metric	Value
LLM-judge vs. clinician triage agreement	14/16 (87.5%)
Cohen’s κ (5-class)	0.808
Model deferrals judged clinically appropriate	3/4 (75%)
Clinician fully agrees with model recommendation	8/16 (50%)
Clinician partially agrees with model	8/16 (50%)
Clinician fully disagrees with model	0/16 (0%)
Clinician deferral rate (this 16-case sample)	6/16 (37.5%)
Model deferral rate (full 60-case corpus)	4/60 (6.7%)

Table 10: Clinician adjudication summary on the $n = 16$ stratified sample. Cohen’s $\kappa = 0.808$ between the LLM-judge majority verdict and the clinician’s primary triage label, on the five-class $\{A, B, C, D, \text{DEFERRED}\}$ scale.

Claim	Reported	Verified
Gemma 3 4B IT L29 per-token L_0 (active features), $n=3950$ tokens	“~35–90 active (median 57)”	median 57.0, mean 58.2, [p5, p95] = [36, 86]
Gemma 3 4B IT L29 per-token residual norm, same sample	“~60,000 per token”	mean 60,583, median 59,433
Intervention: mean norm subtracted per token (case E1, NL)	264	264.4
Intervention: peak norm subtracted on a single token	6,795	6,799.7
Intervention: mean contribution as % of residual norm	~0.4%	0.44%
Intervention: peak contribution as % of residual norm	~11%	10.97%
Gemma Scope 2 4B L29 relative L_2 reconstruction error	~14%	B_mean 14.0%, D_mean 13.6%
Qwen-Scope L31 relative L_2 reconstruction error (L0_100), $n=1663$ tokens	~34%	median 34.4%, mean 37.2%
ActAdd: $\alpha \cdot \ v\ /\ r\ $ at $\alpha=4$	~6.7%	$4 \cdot 1012.66/60,583 = 6.69\%$

Table 11: Verified numerical claims, recomputed end-to-end.

L	Stratum	n	Δ sMAPE [95% CI]	Δ cos [95% CI]
9	both-right	29	-0.232 [-0.265, -0.201]	+0.023 [+0.019, +0.026]
	both-wrong	12	-0.202 [-0.238, -0.167]	+0.024 [+0.019, +0.029]
	NF-only-right	14	-0.213 [-0.241, -0.186]	+0.024 [+0.016, +0.034]
	NL-only-right	1	-0.197 (n=1)	+0.019 (n=1)
	judges_dis.	4	-0.207 [-0.229, -0.190]	+0.026 [+0.020, +0.033]
17	both-right	29	-0.269 [-0.305, -0.231]	+0.035 [+0.023, +0.050] ($n_c=28$)
	both-wrong	12	-0.290 [-0.363, -0.225]	+0.039 [+0.025, +0.056]
	NF-only-right	14	-0.258 [-0.315, -0.205]	+0.027 [+0.017, +0.039] ($n_c=13$)
	NL-only-right	1	-0.206 (n=1)	+0.047 (n=1)
	judges_dis.	4	-0.209 [-0.269, -0.148]	+0.024 [+0.012, +0.041]
22	both-right	29	-0.090 [-0.142, -0.023]	+0.037 [+0.007, +0.061]
	both-wrong	12	-0.093 [-0.175, +0.010]	+0.022 [-0.030, +0.060]
	NF-only-right	14	-0.141 [-0.186, -0.095]	+0.043 [+0.026, +0.058]
	NL-only-right	1	-0.170 (n=1)	+0.050 (n=1)
	judges_dis.	4	-0.141 [-0.211, -0.052]	+0.041 [-0.006, +0.070]
29	both-right	29	-0.275 [-0.329, -0.229]	+0.054 [+0.039, +0.072] ($n_c=24$)
	both-wrong	12	-0.336 [-0.409, -0.265]	+0.060 [+0.025, +0.101] ($n_c=11$)
	NF-only-right	14	-0.338 [-0.402, -0.280]	+0.049 [+0.028, +0.071] ($n_c=12$)
	NL-only-right	1	-0.334 (n=1)	+0.058 (n=1)
	judges_dis.	4	-0.274 [-0.331, -0.217]	+0.075 [+0.031, +0.139]

Table 12: Gemma 3 4B IT — max-pool sMAPE and cosine per stratum at all four analyzed layers. The single NL-only-right case is reported for completeness but excluded from headline claims.

L	Stratum	n	Δ sMAPE [95% CI]	Δ cos [95% CI]
12	both-right	43	+0.009 [-0.026, +0.051]	-0.002 [-0.012, +0.004]
	both-wrong	11	+0.069 [-0.048, +0.222]	-0.020 [-0.067, +0.005]
	NL-only-right	6	+0.020 [-0.125, +0.233]	+0.009 [+0.001, +0.020]
24	both-right	43	+0.233 [+0.183, +0.292]	-0.100 [-0.153, -0.053]
	both-wrong	11	+0.366 [+0.185, +0.589]	-0.110 [-0.183, -0.046]
	NL-only-right	6	+0.429 [+0.311, +0.517]	-0.256 [-0.336, -0.154]
31	both-right	43	-0.222 [-0.241, -0.203]	+0.093 [+0.078, +0.108]
	both-wrong	11	-0.232 [-0.277, -0.189]	+0.094 [+0.067, +0.128]
	NL-only-right	6	-0.262 [-0.312, -0.220]	+0.093 [+0.066, +0.129]
41	both-right	43	-0.110 [-0.136, -0.086]	+0.034 [+0.027, +0.042]
	both-wrong	11	-0.136 [-0.192, -0.083]	+0.035 [+0.023, +0.051]
	NL-only-right	6	-0.200 [-0.278, -0.116]	+0.035 [+0.019, +0.055]

Table 13: Gemma 3 12B IT — max-pool sMAPE and cosine per stratum at all four analyzed layers. The sign of the effect flips between shallow/mid layers (L12, L24, positive sMAPE / negative cosine) and deep layers (L31, L41, negative sMAPE / positive cosine); the two metrics agree on direction at every cell. Per-case values are from the original 12B pipeline run; an independent v2 re-extraction reproduces the same medical feature set ($\{3, 338, 329\}$ at L24, $\{130, 85, 4773\}$ at L31) and every qualitative cell, with small numerical drift ($\leq 5\%$) within bf16 inference non-determinism across GPU instances.

Stratum	n	Δ sMAPE [95% CI]	Δ cos [95% CI]
both-right	29 ($n_c=25$)	-0.285 [-0.340, -0.213]	+0.094 [+0.070, +0.115]
both-wrong	12 ($n_c=11$)	-0.329 [-0.367, -0.290]	+0.108 [+0.085, +0.129]
NF-only-right	14 ($n_c=12$)	-0.272 [-0.345, -0.173]	+0.096 [+0.071, +0.125]
NL-only-right	1	-0.337 (n=1)	+0.114 (n=1)
judges_dis.	4	-0.293 [-0.345, -0.252]	+0.092 [+0.070, +0.127]

Table 14: Restricted random pool at Gemma 3 4B IT L29 (magnitude-matched + firing on $\geq 25\%$ of the 120 NL \cup NF prompts; pool size 3,258 features), max-pool aggregation, on the canonical stratification (F1 in NF-only-right). All populated strata’s 95% CIs exclude zero on both metrics: the medical-vs-restricted-random gap survives the firing-threshold restriction in every stratum, with modest magnitude changes relative to the unrestricted control (Table 12). Per-case random sMAPE/cosine are averaged across 1,000 random draws of 30 features from the restricted pool to stabilize against single-seed sampling variance; the per-case bootstrap CI then propagates through the case-clustered resample ($B=2,000$).

Stratum	n	med. sMAPE	rnd. sMAPE	med. cos	rnd. cos
both-right	35	0.003	0.064	1.000	0.991
NF-only-right	6	0.003	0.124	1.000	0.975
NL-only-right	8	0.002	0.054	1.000	0.994
both-wrong	6	0.004	0.042	1.000	0.994
judges-disagree	5	0.004	0.136	1.000	0.980

Table 15: Qwen3-8B at L31 (L0_100 Qwen-Scope variant) — max-pool sMAPE and cosine per stratum, joined against the Qwen NL-NF correctness labels from the behavioral run (Section 4.1). Medical features stay at near-identical activations under NL-NF across every behavioral stratum (medical sMAPE ≤ 0.005 , cos ≥ 0.9999), while the magnitude-matched random control shows substantially larger format-induced perturbation in every stratum (random sMAPE 0.04–0.14, cos 0.975–0.994). The paired medical–random Δ sMAPE has a bootstrap 95% CI strictly below zero in every populated stratum, matching the per-stratum pattern at 4B and 12B.

Cell	pool	Δ sMAPE	Δ cos
4B L9	mean	−0.219	+0.023
4B L9	max	−0.231	+0.086
4B L17	mean	−0.265	+0.033
4B L17	max	−0.273	+0.074
4B L22	mean	−0.107	+0.036
4B L22	max	−0.139	+0.044
4B L29	mean	−0.303	+0.056
4B L29	max	−0.264	+0.107
12B L12	mean	+0.040	−0.004
12B L12	max	+0.021	−0.005
12B L24	mean	+0.172	−0.093
12B L24	max	+0.277	−0.117
12B L31	mean	−0.238	+0.121
12B L31	max	−0.228	+0.093
12B L41	mean	−0.103	+0.070
12B L41	max	−0.124	+0.034
Qwen L31	mean	−0.064	−0.023 (disagree)
Qwen L31	max	−0.114	+0.010 (agree)

Table 16: Medical–random Δ under mean-pool vs. max-pool across all (model, layer) cells, on both sMAPE and cosine. All cells with $|\Delta| > 0.01$ have 95% bootstrap CIs strictly excluding zero except 12B L12. On Gemma-Scope (JumpReLU) the two metrics agree on direction under *both* aggregations. Only Qwen-Scope (TopK) shows aggregation-sensitivity: under mean-pool, sMAPE reads medical-more-invariant while cosine reads medical-less-similar; under max-pool both metrics agree (medical-more-invariant).

Model	vignette mask med / rnd	full content med / rnd	scaffold (NL) —
4B L29	0.004/0.006	0.004/0.276	—
12B L31	0.003/0.005	0.003/0.123	—
Qwen L31	0.002/0.003	0.026/0.128	—

Table 17: Per-mask sMAPE (medical / random max-pool) for the three headline (model, layer) cells. On the shared vignette mask both medical and random sMAPE collapse to ≈ 0.002 – 0.006 , as expected under causal masking — the vignette-mask sanity check passes. On the full-content max-pool, medical sMAPE remains near zero while random sMAPE rises to 0.12–0.28, the headline medical-random gap.

Cell	med. sMAPE	rnd. sMAPE (5–95%)	perm. p
4B L29	0.004	0.276 [0.138, 0.429]	< 0.001
12B L31	0.003	0.123 [0.072, 0.171]	< 0.001
Qwen L31	0.002	0.218 [0.094, 0.361]	< 0.001

Table 18: 1,000-resample magnitude-matched random control with permutation p -values for the medical-random sMAPE gap at the headline layer per model. The medical-feature sMAPE is below the 5th percentile of the random-pool distribution at every cell; the Qwen row uses the L0_100 Qwen-Scope variant of Section 3.2.

Case	gold	NL	NF (both)	adj.	5-way
4B NF-only-right ($n = 14$, gap-driver)					
E3	C	B	C	✓	—
E4	C	B	C	✓	—
E10	C/D	B	C	✓	—
E11	C/D	B	C	✓	—
E22	C/D	B	C	✓	—
E25	C	B	C	✓	—
F1	C/D	B	C	✓	—
F3	C	B	C	✓	—
F4	C	B	C	✓	—
F10	C/D	B	C	✓	—
F19	B	A	B	✓	—
MH1	C	B	C	✓	—
NH1	C	B	C	✓	—
NH3	C	B	C	✓	—

Table 19: Per-case decomposition of 4B’s NL>NF NF-only-right stratum ($n = 14$). All 14 are single-acuity-step under-triages in NL; 13 follow the exact “NL=B, gold=C, NF→C” pattern. No unanimous DEFERRED cases.

Case	gold	NL	NF (both)	adj.	5-way
12B NL-only-right ($n = 6$, gap-driver)					
E19	B	B	C	✓	—
F3	C	C	B	✓	—
F7	C/D	C	A	×	—
F11	C/D	C	B	✓	—
F13	D	D	C	✓	—
NH3	C	C	D	✓	—
12B unanimous DEFERRED (all in both-right)					
F15	C/D	C	B	—	DEF
F19	B	B	B	—	DEF
F23	A/B	B	B	—	DEF
F24	B	B	B	—	DEF

Table 20: 12B’s NL>NF NL-only-right stratum ($n = 6$, 5 adjacent miscalibrations) and the four unanimous DEFERRED cases. The deferrals flatten to gold-compatible letters and live in both-right, contributing zero to the gap.

Case	gold	NL	NF (both)	adj.	5-way
Qwen NL-only-right ($n = 8$)					
E3	C	C	B	✓	—
E4	C	C	B	✓	—
E8	A	A	B	✓	—
E17	A	A	B	✓	—
F1	C/D	C	B	✓	—
F4	C	C	B	✓	—
F11	C/D	C	B	✓	—
F25	C	C	D	✓	—
Qwen NF-only-right ($n = 6$)					
E6	B/C	A	C	×	—
E7	C/D	A	C	×	—
F6	B/C	A	C	×	—
F7	C/D	A	C	×	—
F10	C/D	A	C	×	—
F24	B	A	B	✓	—

Table 21: Qwen3-8B has both strata at lower magnitude. The NL-only-right stratum is 8/8 adjacent miscalibrations. The NF-only-right stratum exhibits a distinctive 2-step NL=A under-triage pattern on 5/6 cases.

Signal	4B	12B	Qwen
K=23 exhaustive (case-clustered 95% CI)			
Same-letter (chance 25%)	22.4 [21.4, 23.4]	20.8 [18.6, 23.0]	23.3 [20.5, 26.5]
Same-content (chance 25%)	64.5 [55.9, 73.0]	80.3 [73.6, 86.6]	82.6 [76.2, 88.4]
Shuffled NL acc	69.8 [60.7, 78.3]	76.3 [66.3, 85.3]	75.4 [66.0, 84.5]
Canonical NL acc	55.0%	81.7%	75.0%
NF (free-text) acc	71.7%	71.7%	68.3%
Shuffled – NF (pp)	–1.9 (ns)	+4.6	+7.1
Picks “ER now” content	2/1380 (0.14%)	126/1380 (9.1%)	97/1380 (7.0%)

Table 22: Exhaustive option-order shuffle (60 cases \times all 23 non-identity permutations of A–D label assignments per case, per model, 4140 forward passes total). The same-letter rates’ case-clustered 95% CIs exclude the 25% chance baseline at 4B and 12B and contain it at Qwen, ruling out position bias at every scale. The same-content rates are far above chance at every model, isolating a strong content prior. At 4B shuffled forced-letter accuracy (69.8%) is *statistically indistinguishable* from NF accuracy (71.7%): the entire NL-NF gap at 4B is consistent with a canonical answer-key-mapping artifact. At 12B and Qwen, the canonical mapping is approximately neutral but shuffled NL still beats NF by ~ 5 –7pp, indicating a separate NF-mode adjacent-miscalibration does not remove. Capability scaling shows up in the “ER now” row: 4B almost never recommends ER even when the label is favorable (0.14%), while 12B and Qwen do so 7–9% of the time. (For comparison, the K=3 random subsample reported in an earlier draft happened to yield exactly 71.7% shuffled NL at 4B; the exhaustive K=23 estimate of 69.8% is the precise value with a 95% CI containing NF.)

Model	Category	abs-fraction (5–95% CI)	margin-share (5–95% CI)
4B L29	medical (3 feats)	0.0%	0.0%
	scaffold (top 30)	0.1% [0.0, 0.4]	0.1% [-0.4, 1.0]
	other (~47 feats)	99.9% [99.6, 100.0]	99.9% [99.0, 100.4]
12B L31	medical (3 feats)	0.0%	0.0%
	scaffold (top 30)	50.3% [45.6, 54.9]	26.5% [-27.4, 63.6]
	other (~47 feats)	49.7% [45.1, 54.4]	73.5% [36.4, 127.4]

Table 23: Decision-token logit attribution at the NL pre-generation token. *abs-fraction* is each category’s absolute linear effect on A/B/C/D logits (as a fraction of the total absolute effect across all features); *margin-share* is its signed contribution to the predicted-vs-runner-up margin. The linear projection ignores final LayerNorm, later transformer layers, and SAE reconstruction error, so magnitudes are approximate. The categorical result is stable: the three medical features contribute zero, consistent with zero activation in 60/60 cases.

Model	NL∩NF top-20 (Jaccard)	NL-only peak on B scaffold	NF-only peak on D vignette
4B L29	0.000 [0.00, 0.00]	87.0% (med. 90%)	27.8%
12B L31	0.001 [0.00, 0.00]	88.3% (med. 90%)	8.9%
Qwen L31	0.324 [0.25, 0.38]	94.7% (med. 100%)	10.4%

Table 24: Decision-token top-20 feature characterization. At Gemma the NL and NF top-20 sets are disjoint (Jaccard ≈ 0); at Qwen they share about a third. Across all three models, 87–95% of features unique to NL’s top-20 peak on B-prompt scaffold tokens outside the shared vignette — the direct quantification of “scaffold-primary at NL.” Features unique to NF’s top-20 peak on D-prompt vignette tokens only 8–28% of the time, indicating that “content-primary at NF” is weaker than the NL-side scaffold finding; many NF-only top-20 features peak elsewhere on the D prompt (e.g. closing punctuation, question-mark tokens).

Model / Layer	med sMAPE	rnd sMAPE	paired Δ [95% CI]	Sig
4B L29	0.0042	0.0827	-0.0810 [-0.096, -0.066]	*
12B L31	0.0025	0.0692	-0.0618 [-0.083, -0.034]	*
Qwen L31	0.0020	0.1126	-0.1501 [-0.183, -0.117]	*

Table 25: SL-SF mechanistic invariance at the headline layer per model. Δ = medical–random sMAPE; lower = more invariant. * marks cells whose bootstrap 95% CI excludes zero. Vignette-mask sanity check (shared-content sMAPE ≈ 0.002 – 0.006 for both pools across all three models) confirms causal-masking-trivial invariance.